Enhancing High-Resolution Forest Stand Mean Height Mapping in China through an Individual Tree-Based Approach with Close-Range LiDAR Data

Yuling Chen[1],[★], Haitao Yang[1],[★], Zekun Yang[1], Qiuli Yang[2,3], Weiyan Liu[4], Guoran Huang[5], Yu Ren[1], Kai Cheng[1], Tianyu Xiang[6], Mengxi Chen[1], Danyang Lin[4], Zhiyong Qi[1], Jiachen Xu[1], Yixuan Zhang[1], Guangcai Xu[7], Qinghua Guo[1,8*]

[1]Institute of Remote Sensing and Geographic Information System, School of Earth and Space Sciences, Peking University, Beijing 100871, China
[2]College of Geography and Remote Sensing Science, Xinjiang University, Urumqi 800017, China
[3]Xinjiang Key Laboratory of Oasis Ecology, Xinjiang University, Urumqi 830017, China
[4]State Forestry and Grassland Administration Key Laboratory of Forest Resources & Environmental Management, Beijing Forestry University, Beijing 100083, China
[5]College of Forestry, Southwest Forestry University, Kunming 650224, China
[6]College of Earth Sciences, Chengdu University of Technology, Chengdu 610059, China
[7]Beijing GreenValleyTechnology Co., Ltd, HaidianDistrict, Beijing 100091, China
[8]Institute of Ecology, College of Urban and Environmental Sciences, Peking University, Beijing 100871, China

[★]These authors contributed equally to this work.

Correspondence to: Qinghua Guo (guo.qinghua@pku.edu.cn)

Abstract. Forest stand mean height is a critical indicator in forestry, playing a pivotal role in various aspects such as forest inventory, sustainable forest management practices, climate change mitigation strategies, monitoring of forest structure changes, and wildlife habitat assessment. However, there is currently a lack of large-scale, spatially continuous forest stand mean height maps. This is primarily due to the requirement of accurate measurement of individual tree height in each forest plot, a task that cannot be effectively achieved by existing globally covered, discrete footprint-based satellite platforms. To address this gap, this study was conducted using over 1117 km^2 of close-range Light Detection and Ranging (LiDAR) data, which enables the measurement of individual tree height in forest plots with high precision. Besides, this study incorporated spatially continuous climatic, edaphic, topographic, vegetative, and Synthetic Aperture Radar data as explanatory variables to map the tree-based arithmetic mean height (h_a) and weighted mean height (h_w) at 30 m resolution across China. Due to limitations in obtaining basal area of individual tree within plots using UAV LiDAR data, this study calculated weighted mean height through weighting an individual tree height by the square of its height. In addition, to overcome the potential influence of different vegetation divisions at large spatial scale, we also developed a machine learning-based mixed-effects model to map forest stand mean height across China. The results showed that the average h_a and h_w across China were 11.3 m and 13.3 m with standard deviations of 2.9 m and 3.3 m, respectively. The accuracy of mapped products was validated utilizing LiDAR and field measurement data. The correlation coefficient (r) for h_a and h_w ranged from 0.603 to 0.906 and 0.634 to 0.889,

while RMSE ranged from 2.6 to 4.1 m and 2.9 to 4.3 m, respectively. Comparing with existing forest canopy height maps derived using the area-based approach, it was found that our products of h_a and h_w performed better and aligned more closely with the natural definition of tree height. The methods and maps presented in this study provide a solid foundation for estimating carbon storage, monitoring changes in forest structure, managing forest inventory, and assessing wildlife habitat availability. The dataset constructed for this study is publicly available at https://doi.org/10.5281/zenodo.12697784 (Chen et al., 2024).

1 Introduction

Tree height is a pivotal indicator in forestry (Wang et al. 2019a), with paramount importance for forest inventory, wildlife habitat assessment and climate change mitigation strategies (Vaglio Laurin et al. 2019; Wang et al. 2019b; Zemp et al. 2023). Forest stand height denotes the mean height of trees within a stand/plot, including arithmetic mean height and mean height weighted in proportion to their basal area (weighted mean height or Lorey's mean height) (Laar and Akça 2007; Masaka et al. 2013). It serves as a key factor in assessing forest growth (Ma et al. 2023; McGregor et al. 2021), calculating forest volume (Xu et al. 2019) and carbon storage (Yao et al. 2018), as well as guiding sustainable forest management practices (Xu et al. 2023). Nevertheless, traditional tree height measurements derived from field surveys are typically time-consuming and resource-intensive (Jurjević et al. 2020; Liu et al. 2022), making it impractical to generate comprehensive wall-to-wall forest stand mean height data products across extensive spatial scales (Su et al. 2017). Although passive remote sensing techniques offer a potential solution for estimating forest stand height indirectly (Donoghue and Watt 2006; Hall et al. 2006; Lu et al. 2004; Zhang et al. 2014). They are constrained by penetration ability and saturation effects, resulting in inherent uncertainty issues (Liu et al. 2022; Su et al. 2015). Mapping high-resolution forest stand mean height at a large scale through individual tree-based measurements remains a challenging but crucial objective in forest management and ecosystem monitoring.

Light detection and ranging (LiDAR), utilizing focused wavelength laser pulses, is an active remote sensing technique renowned for its robust penetration ability to directly characterize three-dimensional structures of forest (Guo et al. 2021; Liang et al. 2022; Liu et al. 2022; Ma et al. 2023; Su et al. 2017). The development of multi-platforms LiDAR scanning has greatly enhanced the precision of tree height measurement from the individual trees to regional scales (Guo et al. 2021; Jurjević et al. 2020; Liu et al. 2022; Wang et al. 2019a). Additionally, to address challenges in accuracy and cost of LiDAR data, the innovations in close-range LiDAR, particularly through the use of unmanned aerial vehicles (UAVs) and terrestrial laser scanning, have enhanced the flexibility, accessibility and cost-effectiveness of LiDAR data in forestry applications (Guo et al. 2021; Hu et al. 2021; Yin et al. 2024). Consequently, the advancement of close-range LiDAR has laid a robust foundation of data and technology, facilitating the high-resolution wall-to-wall tree height mapping at large spatial scales.

Two main approaches are utilized for tree height measurement with LiDAR data: area-based approach (Bouvier et al. 2015; Liu et al. 2022); and tree-based approach (Su et al. 2017; Swayze et al. 2021; Yin et al. 2024). These approaches differ in their definition of "height" and the method used for calculation. The area-based approach, also known as the grid-based approach,

simplifies the process of obtaining tree height. It involves generating a canopy height model (CHM) to calculate tree height based on the statistical relationships between plot-level LiDAR metrics. The height metrics obtained from this approach is

70   forest canopy height, which include not only the actual tree height, but also the height of other branches (Bouvier et al. 2015). Additionally, changes of in height within non-tree or non-vegetation pixels may also be included, leading to further deviation from the definition of tree height in forestry (Yin et al. 2024). Tree height calculated from the tree-based approach closely aligns with to the natural definition of tree height, which the height being evaluated is the height from individual tree, ranging from the treetop to the ground. This approach requires first detecting individual trees in a sample plot, the measuring the height

75   of each tree in this plot, and finally calculating forest stand height (Laar and Akça 2007; Masaka et al. 2013). Data from close-range LiDAR, with its advanced algorithms for individual tree segmentation, is widely used in the tree-based approach (Li et al. 2012; Qin et al. 2022; Tao et al. 2015; Yang et al. 2020; Yang et al. 2024; Yun et al. 2021). Despite its wide use in small-scale areas or specific forest types (Jurjević et al. 2020; Kwong and Fung 2020; Næsset and Økland 2002; Su et al. 2017; Yin et al. 2024), research gaps remain regarding large scale application of the tree-based approach. Moreover, the absence of large-

80   scale forest stand height metrics derived from the tree-based approach hinders the comparisons between tree-based and area-based methods for tree height estimation. Thus, to effectively implement sustainable management and development practices that balance conservation and human use needs, it is crucial to have comprehensive, timely, and accurate inventory and monitoring efforts for the height of forests at a national scale (Coops et al. 2021; Liu et al. 2022; Travers-Smith et al. 2024). However, there are challenges associated with using close-range LiDAR to collect continuous large-scale forest stand height

85   observations considering the sparse coverage of LiDAR data and the associated costs.

To overcome the spatial discontinuity problem of close-range LiDAR samples on a large spatial scale, integration of multiple types of remote sensing data is a commonly used method for mapping wall-to-wall forest height (Huang et al. 2017; Lefsky 2010; Lefsky et al. 2005; Liu et al. 2022; Su et al. 2017; Travers-Smith et al. 2024). Current approaches typically rely on spatial interpolation and regression techniques. Spatial interpolation involves predicting values at unobserved locations based

90   on observed data points (Allard, 2013), taking advantage of spaceborne LiDAR data in wall-to-wall maps across extensive geographic areas with high resolution (Liu et al. 2022). For example, Liu et al. (2022) developed a spatial interpolation method to map China's forest canopy height by fusing GEDI, ICESat-2 ATLAS, and Sentinel-2 images. When it comes to forest stand mean height mapping, the spatial interpolation method may not be the most suitable method due to the rarity of forest stand mean heights in current spaceborne systems. In contrast, the regression strategy utilizes the continuous characteristics of optical

95   remote sensing, radar, and existing data products as predictors to construct non-linear mathematical models linking environmental factors with observations. For example, Su et al. (2017) used the random forest algorithm to model forest stand height in Sierra Nevada based on GLAS tree heights, optical imagery, topographic data and climate information. Travers-Smith et al. (2024) combined LiDAR and optical remote sensing products to map vegetation in high latitudes with a high overall accuracy. Currently, machine learning (ML) algorithms (Cheng et al. 2024a; Cheng et al. 2024b; Coops et al. 2021;

100   Matasci et al. 2018) and deep learning algorithms (Fayad et al. 2024; Liu et al. 2022) are the primary non-linear mathematical regression approaches for achieving large-scale continuous spatial forest attributes mapping. Compared to deep learning

algorithms, ML algorithms based on structured data are easier to implement and less computationally intensive. More importantly, in the context of mapping forest stand heights, feature engineering to compute relevant vegetation metrics is often preferred over utilizing raw radar and optical remote sensing data (Li et al. 2020; Potapov et al. 2021). Therefore, for estimation the forest stand height through a tree-based approach at large scale, the regression strategy using ML algorithms provides a robust solution for integrating multi-source remote data for wall-to-wall forest stand height mapping.

Variations in forest types within different vegetation divisions on large spatial scales may also influence the accuracy of forest stand height mapping. One feasible solution is to develop specific model for each ecozone (Wu and Shi 2023). However, this approach may lead to noticeable boundary effects when estimating results based on multiple specific models. Therefore, addressing how to adequately account for the spatial differences on a large spatial scale while using a single-global model is a problem that requires to be solved. The mixed-effects model, as demonstrated by Choi et al. (2024), offers a potential solution to simultaneously consider the heterogeneities of different regions. By integrating the mixed-effects model with ML, as proposed by Hu and Szymczak (2023), one can effectively leverage the strengths of both approaches to address complex data analysis challenges. This combination allows for the consideration of both random and fixed effects in the data while harnessing the flexibility and non-linear mathematical regression of ML to better explain the complexity of the data.

In this study, our main objective is to map the national scale forest stand mean height across China through machine learning. We aim to address the challenges and potential for continuous mapping of tree height in heterogeneous forest ecosystem, through a tree-based approach. To train machine learning models, we have collected over 1117 km^2 of UAV LiDAR data across China. Subsequently, we mapped two forest stand mean height products at 30 m resolution: the arithmetic mean height (h_a) and the weighted mean height (h_w). Furthermore, we have validated the resulting forest stand mean height products by comparing them with field measurements and UAV LiDAR validation data. The national-scale maps of forest stand mean height produced in this study hold various applications, including estimating forest inventory, developing climate change mitigation strategies, monitoring changes in forest structure, and assessing wildlife habitat.

2 Material and methods

As illustrated in Figure 1, the workflow for this study involved four main steps: (1) Close-Range LiDAR data processing, including individual tree segmentation and forest stand mean height calculation, (2) Feature set construction, including multi-source remote sensing data and ancillary data processing, (3) ML-based mixed-effects (MLME) modeling, (4) Mapping of wall-to-wall forest stand mean height across China, including accuracy assessment and uncertainty analysis.
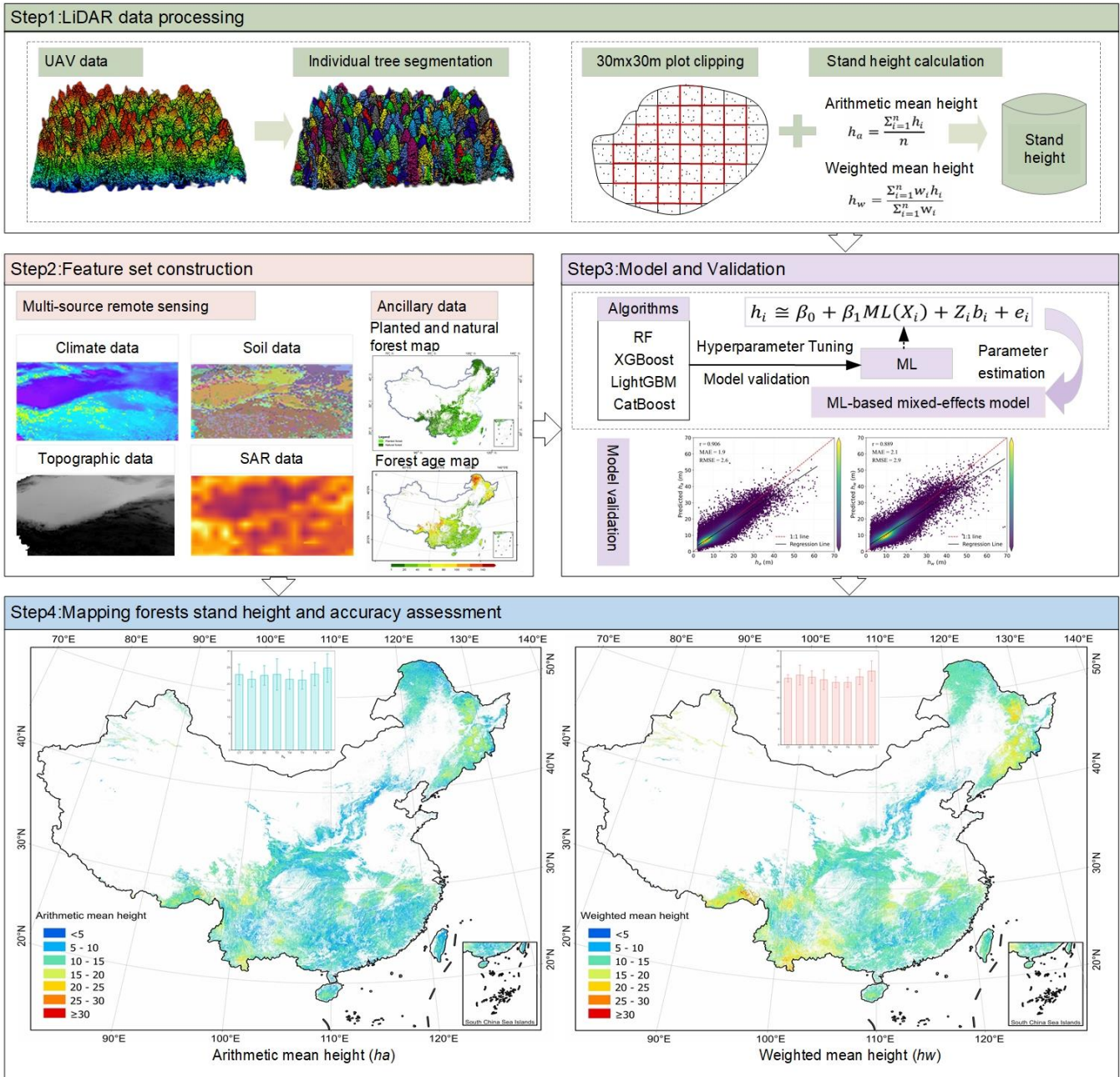
Figure 1: Workflow adopted for the modeling and mapping forest stand mean heights (h_a and h_w) at 30 m resolution across the China's forest. Publisher's remark: please note that the above figure contains disputed territories.

2.1 Close-range LiDAR data

The close-range LiDAR data used in this study were collected since 2015, covering various types of vegetation divisions across China, excluding the Qinghai-Tibet Plateau alpine vegetation divisions (Table 1, 2 and Fig. 2). The UAV LiDAR system was

utilized in this study, resulting in a total data volume of 400 TB and covering an area of 1117.76 km^2 (Table 2 and Fig. 2).
These data serve as the foundation for creating the forest stand mean heights sample set. The LiDAR data underwent initial
processing using LiDAR360 software (V 6.0, www.lidar360.com), which included resampling, denoising, ground point
classification, and normalization. The processed LiDAR data were then partitioned into 30×30 m grids, representing plots or
stands of forest. In total, there were 610,342 plots created. To identify individual trees with height attribute within 30×30 m
plots, the individual tree segmentation algorithm (Li et al. 2012) was introduced through the LiDAR360 software that designed
for Manned/UAV LiDAR data. Manual visual inspection was conducted for each plot to determine the optimal parameters for
individual tree segmentation within the LiDAR360 software, ensuring more precise and reliable results. The dataset was used
to train and validated the maps of forest stand mean heights in this study.

Table 1. LiDAR sensor parameter information during 2015 and 2023.

LiDAR sensor	MAX points per second (pts/s)	Wave length	Range accuracy	Point density (pts/m²)	Product
Pandar40P	1,440,000(dual return)	905 nm	2 cm	2061	LiAir 220N
Riegl mini VUX-1UAV	100,000	Near Infrared	1.5 cm	14	LiAir 250
XT32M2X	1,920,000(triple return)	905nm	1.0 cm	2747	LiAir 300
Riegl VUX-1LR-22	1,500,000	Near Infrared	1.5 cm	207	LiAir D1350
Riegl VUX-1LR-22	1,500,000	Near Infrared	1.5 cm	207	LiAir E1350
Riegl VUX-120-23	2,400,000	Near Infrared	1.0 cm	1049	LiAir E1500
Riegl VUX-1LR-22	1,500,000	Near Infrared	1.5 cm	207	LiAir H2.0
Riegl VUX-120-23	2,400,000	Near Infrared	1.0 cm	1049	LiAir H1500
Riegl VUX-1LR-22	1,500,000	Near Infrared	1.5 cm	207	LiAir H1800
Livox Horizon	240,000	905 nm	2.0 cm	145	LiAir VH
Livox Mid-40	100,000	905 nm	2.0 cm	150	LiAir V
Livox AVIA	720,000(triple return)	905 nm	2.0 cm	536	LiAir V70
Livox AVIA	720,000(triple return)	905 nm	2.0 cm	536	LiAir VH2
Velodyne's Puck	600,000(dual return)	903 nm	3.0 cm	1166	LiAir 50N
Riegl VUX-1LR-22	1,500,000	Near Infrared	1.5 cm	207	LiHawk

Note: We calculated point density (pts/m²) based on terrain-following mode. The UAV LiDAR sensor maintained a height of
120 m above the ground, flew at a speed of 8 m/s, and had a forward overlap ratio of 70% and a lateral overlap ratio of 30%.

Table 2. Summary of the collected UAV LiDAR data grouped in eight vegetation divisions across China.

Vegetation division	Total area (km^2)	Proportion of forest area covered by drone lidar data ($\times 10^{-5}$)
Temperate desert (TD)	0.18	0.75
Temperate steppe (TS)	76.04	98.16
Subtropical evergreen broadleaf forest (SE)	755.91	54.28
Tropical monsoon forest-rainforest (TM)	65.42	39.64
Warm temperate deciduous broadleaf forest (WT)	163.97	74.92
Temperate needleleaf-broadleaf mixed forest (TN)	53.61	19.46
Cold temperate needleleaf forest (CT)	2.63	1.16

Notes: Proportion of forest area covered by lidar data is the value the ratio of the area where data was collected to the forest area in each vegetation division.
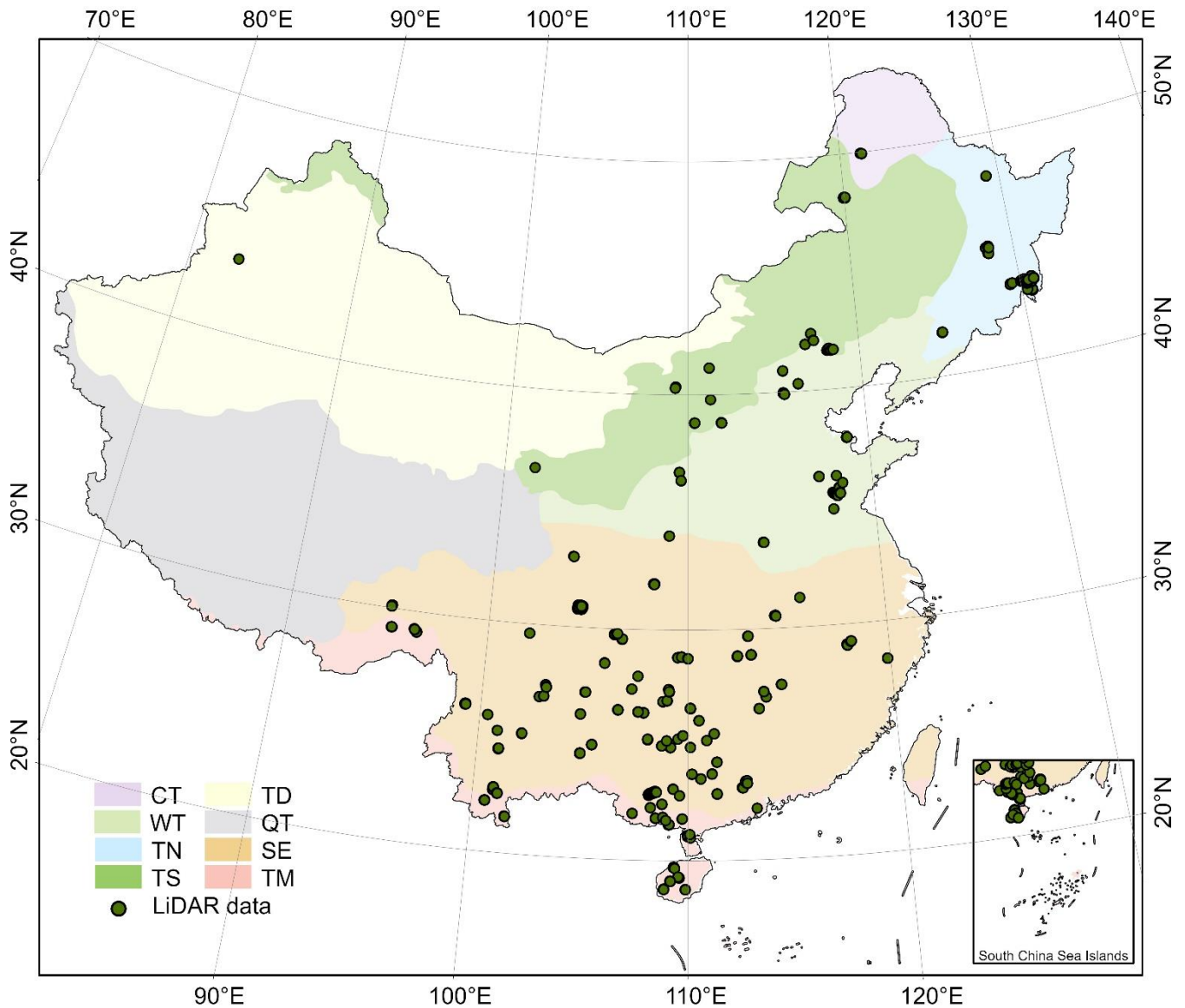
Figure 2: Spatial distribution of the close-range LiDAR data used in this study. CT, TN, TS, TD, WT, QT, SE, and TM represent the vegetation divisions of cold temperate needleleaf forest, temperate needleleaf-broadleaf mixed forest, temperate steppe, temperate desert, warm temperate deciduous-broadleaf forest, Qinghai-Tibet Plateau alpine vegetation, subtropical evergreen broadleaf forest, and tropical monsoon forest-rainforest, respectively. Publisher's remark: please note that the above figure contains disputed territories.

2.2 Field data

Field samples were collected for weighted mean height calculation (see Section 2.3) and product validation (see Section 2.5). From 2019 to 2023, a total of 294 plots were collected in six provinces of China. All of the plots achieved decimeter-level positioning accuracy, and each plot covered an area larger than 400 m². The center position and information of individual trees

in each plot, including DBH (DBH > 5 cm) and tree height were recorded in each plot. However, it is worth noting that there

165 may exists the time discrepancy between the field surveys and LiDAR data acquisition. Additionally, variability may be introduced due to multiple field surveyors and region-specific adjustments to measurement tools.

2.3 Tree-based approach for calculating Forest stand mean heights

Forest stand mean heights, including h_a and h_w, were calculated using a tree-based approach in this study (Laar and Akça 2007; Nakai et al. 2010). While accurately segmenting individual trees based on LiDAR data might be challenging due to

170 missing smaller trees and trees obscured by understory vegetation (Li et al. 2012; Tao et al. 2015; Yang et al. 2024), leading to some under-segmentation, this step remains crucial for modeling and mapping forest stand mean heights. Therefore, in this study, we only considered the parameter extraction of successfully segmented trees when using the tree-based approach for the inverting and mapping forest stand mean heights. The segmented individual tree results obtained from close-range LiDAR data contained latitude, longitude, and tree height information for each tree.

175 **2.3.1 Arithmetic mean height** *(h_a)*

The arithmetic mean height (h_a) is calculated as the average of the tree heights of all trees obtained from the 30×30 m plots basing on our UAV LiDAR data. It is calculated as following:

$$h_a = \frac{\Sigma_{i=1}^{n} h_i}{n} \tag{1}$$

where h_i is the height of *i-th* tree (usually with a threshold of $h_i \geq 2.0$ m), *n* is the number of trees within the grid.

2.3.2 Weighted mean height *(h_w)*

180 Weighted mean height (h_w) is calculated by using the basal area as the weight for determining the forest stand mean height (Laar and Akça 2007; Lorey 1878; Masaka et al. 2013). It is calculated as following:

$$h_w = \frac{\Sigma_{i=1}^{n} w_i h_i}{\Sigma_{i=1}^{n} w_i} \tag{2}$$

where h_w represents the weighted mean height (m), h_i is the height of *i-th* tree (usually with a threshold of $h_i \geq 2.0$ m), w_i is the weight (basal area) of *i-th* tree, *n* is the number of trees within the plot or stand.

Considering the limitations in obtaining basal area of individual trees within plots using UAV LiDAR data, the basal area

185 cannot be used as a weight for calculating h_w in this study. According to Næsset (1997), since the basal area of a tree is closely correlated to its height, the value of an individual tree height can be weighted by its tree height or even by the square of its height. Therefore, in this study, we adopted Næsset (1997) method to calculate h_w, taking the tree height (w_1) and square of tree height (w_2) as two alternative weights. The results were compared with the h_w weighted based on basal area, the better-performing one was selected as the final weight in this study. To determine the optimal weight, theoretical growth equations

190 (Supplementary Table S1) for stand age and Lorey's mean height (h_L, based on basal area) were constructed employing

national forest inventory data (Cheng et al. 2024a). The optimal logistic model was selected as the stand age - h_L model (Supplementary Table S2 and S3). Then, close-range LiDAR data and forest age data from Cheng et al. (2024a) were combined with the selected model to calculate $\hat{h}_L$ weighted by basal area. In addition, h_{w1} and h_{w2} were calculated based on weights of w_1 and w_2, respectively. The errors between $\hat{h}_L$ and the two weighted mean heights (h_{w1} and h_{w2}) were derived and the one

195 with smaller error were selected as the weighted mean height h_w for this study (Supplementary Table S4). Finally, to confirm the accuracy of the selected weighted h_w from the second step, it was compared with the basal area-weighted h_L of 199 sample plots, calculated using integrated LiDAR and field data (including manually measured DBH and LiDAR-measured tree heights for each plot). h_w weighted by w_2 showed a strong correlation with h_L, with $r = 0.92$, RMSE = 1.8 m and MAE = 1.0 m (Fig. 3 and Supplementary Table S4). Thus, in this study, w_2 was used as the weight in the calculation of h_w.

200
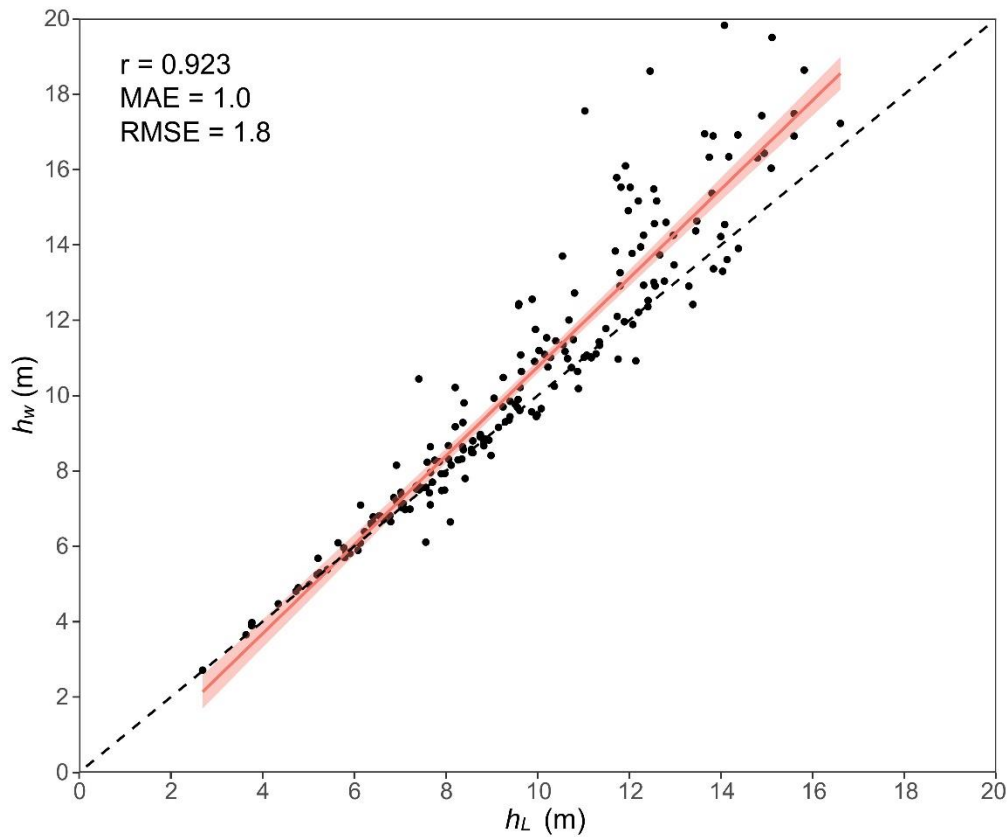
Figure 3: The scatter plot for correlation analysis between h_w (weighted by its square of tree height) and h_L

2.4 Ancillary data

In order to invert the forest stand mean height across China, 30 geospatial features were derived from multi-source remote sensing data. These features were grouped into five categories: climatic, edaphic, topographic, vegetative, and SAR data as

205 shown in Table 3. Climate data were obtained from WorldClim 2.1 (www.worldclim.org), which provides 19 bioclimatic

variables including temperature and precipitation at a 30 arc-second resolution. The Harmonized World Soil Database (HWSD) V1.2, with a resolution of 30 arc-second, was used to extract soil factors, including soil type and soil texture, to construct the tree density estimation model. The Shuttle Radar Topography Mission (SRTM) V3 product (SRTM Plus) provides global digital elevation data at 1 arc-second resolution and was used to extract topographic features. Three topographic features, i.e.,

210 elevation, slope, and aspect, were calculated using the Python *ee* package in this study (Table 3). The vegetative index used in this study is the Landsat-based annual maximum composite Normalized Digital Vegetation Index (NDVI) obtained from the Google Earth Engine (GEE). The SAR data, including VV and VH, were derived from Sentinel-1. The planted and natural forest map was used to separate natural forests from planted ones (Cheng et al. 2024b). Additionally, the forest age map for China in 2020 (Cheng et al. 2024a) was utilized. For consistency, all geospatial features were resampled to a 30 m resolution

215 using the nearest resampling method.

Table 3. Descriptions of multi-source remote sensing variables used to map China's forest stand mean heights product.

Data type	Data source	Resolution	Time	Variables
Forest mask	Planted and natural forest map (Cheng et al.,2023b)	30m	2020	Planted and natural forest
Forest age	Forest age map (Cheng et al.,2023a)	30m	2020	Forest age
SAR data	Sentinel-1	30m	2015–2020	VV, VH
Landsat data	Landsat	30m	2015–2020	NDVI_MAX
Climate data	WorldClim V2.1	30 arc-second	1970–2000	BIO1-BIO19
Soil data	Harmonized World Soil Database V1.2	30 arc-second	2007–2009	SU_SYM90, REF_DEPTH, T_TEXTURE
Topographic data	SRTM DEM	30 m	2000	Elevation, Slope, Aspect

2.5 ML-based mixed-effects model to map wall-to-wall forest stand mean height of China

The modeling data of the study have a hierarchical structure, including eight vegetation divisions, each hosting its specific plots. It is noteworthy that plots within the same vegetation division are not independent, and they exhibit notable heterogeneity when compared across various vegetation divisions. To address the problems, we proposed a novel machine learning-based

220 mixed-effects model framework. It integrates machine learning algorithms with mixed-effects model methodology, providing a powerful and flexible solution for modeling heterogeneous hierarchical data. This method not only enhances the accuracy of modeling, but also provides in-depth results for studies with complex data structures.

2.5.1 ML-based mixed-effects model (MLME)

225   We assumed there are n vegetation divisions, each containing forest stand mean height measurements taken at m spatial points. These spatial points correspond to 30×30 m plots in this study. We denote the t-th ($t = 1, 2, ..., m$) plot measurement in the i-th ($i = 1, 2, ..., n$) vegetation division as h_{it}. The means, variances, and correlations of the forest stand mean height within the n vegetation divisions in each given plot, can be expressed as.

$$\mu = \begin{bmatrix} \mu_1 \\ \mu_2 \\ \vdots \\ \mu_m \end{bmatrix} \quad \sigma^2 = \begin{bmatrix} \sigma_1{}^2 \\ \sigma_2{}^2 \\ \vdots \\ \sigma_m{}^2 \end{bmatrix} \quad CORR = \begin{bmatrix} 1 & \rho_{12} \cdots & \rho_{1m} \\ \rho_{21} & 1 \cdots & \rho_{2m} \\ \vdots & \vdots \; \vdots & \vdots \\ \rho_{m1} & \rho_{m2} \cdots & 1 \end{bmatrix} \tag{3}$$

A non-linear mean function was chosen.

$$\mu_t \cong f(X_t; \beta), t = 1, 2, ..., \text{m} \tag{4}$$

230   where β is the parameter vector, X_t is predictor variables at plot t.

With the addition of certain random effects to the base model of Equation. 4, a nonlinear mixed-effects model of general form is obtained.

$$h_i = f(X_i; \beta, b_i) + \varepsilon_i, i = 1, 2, ..., n \tag{5}$$

where f denotes the forest stand mean height function, h_i is the forest stand mean height at the i-th vegetation division, β is the population parameter vector that is common to all vegetation divisions, and b_i is the random-effect vector specific to the

235   i-th vegetation division, the ε_i is the error term.

To utilize linear prediction, we incorporate the random effects b_i to linearize model (Equation 5) with respect to the random effects as shown in Equation 6. This model, linear in random effects, is termed a nonlinear marginal model (Demidenko 2013; Wang et al. 2023).

$$h_i \cong f(X_i; \beta) + Z_i b_i + \varepsilon_i, i = 1, 2, ..., n \tag{6}$$

where Z_i is the matrix of first-order derivatives with respect to the random effects.

240   The model described in Equation 6 is decomposed into two distinct components: one related to fixed effects and the other related to random effects. For the fixed effect functions, we employed ML models, proposing the MLME model as described in Equation 7.

$$h_i \cong \beta_0 + \beta_1 ML(X_i) + Z_i b_i + \varepsilon_i, i = 1, 2, ..., n \tag{7}$$

where $ML(X_i)$ represents the predicted value from the ML of each plot t (= 1, 2, ..., m) within the mixed-effects model for vegetation division i (= 1, 2, ..., n). β_0 denotes the intercept coefficient and β_1 is the coefficient for the vector of predicted value for $ML(X_i)$. By using the predicted values from ML model, the influence of covariates is integrated into the mixed-effects model, thereby accounting for the specific forest stand mean height measurement within vegetation divisions.

2.5.2 Mapping wall-to-wall forest stand mean heights across China

According to workflow outlined in section 2.5.1, our work began with building the ML models to determine the fixed effects. We employed *PyCaret,* an open-source, low-code ML library in Python (https://pycaret.org), which integrates various popular ML libraries and frameworks, to select ML algorithms for forest stand mean height estimation. Four ML algorithms, including random forest (RF), eXtreme Gradient Boosting (XGBoost), Light Gradient Boosting Machine (LightGBM), and Categorical Boosting (CatBoost), demonstrated superior performance (Supplementary Table S5). Then, the Bayesian optimization was employed for hyperparameter tuning (Mekruksavanich et al. 2022), using *Optuna*, an open-source framework for hyperparameter optimization, to automate the search for hyperparameters (Akiba et al. 2019) (Supplementary Table S6 and S7). Next, the parameters of MLME were estimated using a two-step procedure. First, the forest stand mean height models were trained using the four ML algorithms to obtain h_a and h_w. It was found that LightGBM demonstrate the optimal performance and was selected to map h_a and h_w across China (Supplementary Table S8). Secondly, Equation 7 in section 2.5.1 was applied to derive vegetation division-specific estimates of heights based on the forest stand mean height obtained from these best LightGBM models. Specifically, the *lmer* function from the *lme4* package in the R language (version 4.3.0) was used for maximum likelihood estimation during model fitting.

2.5.3 Accuracy assessment

The original dataset was randomly split into two groups: 2/3 for the training set, and the remaining for the validation set. Several statistical indicators, including coefficient of determination (R^2), root mean square error (RMSE), relative root mean square error (rRMSE), mean square error (MSE), and mean absolute error (MAE) were calculated to evaluate the performance of the ML model in this research. Additionally, Akaike information criterion (AIC) and Bayesian information criterion (BIC) were employed to compare the accuracy and generalization of the parameter estimation results of the MLME model. The Intraclass Correlation Coefficient (ICC) is a statistical measure used to quantify the reliability or agreement of measurements made by multiple plot observers measuring the same vegetation division. These statistical indicators are defined as follows:

$$R^2 = 1 - \frac{\sum_{i=1}^{n}(y_i - \hat{y}_i)^2}{\sum_{i=1}^{n}(y_i - \overline{y})^2} \tag{8}$$

$$MSE = \frac{1}{n}\sum_{i=1}^{n}(y_i - \hat{y}_i)^2 \tag{9}$$

$$RMSE = \sqrt{\frac{1}{n}\sum_{i=1}^{n}(y_i - \hat{y_i})^2} \tag{10}$$

$$rRMSE = \frac{\sqrt{\frac{1}{n}\sum_{i=1}^{n}(y_i - \hat{y_i})^2}}{\overline{y}} \times 100\% \tag{11}$$

$$MAE = \frac{1}{n}\sum_{i=1}^{n}\left|y_i - \hat{y_i}\right| \tag{12}$$

$$ICC = \frac{\hat{\sigma_b}^2}{\hat{\sigma_b}^2 + \hat{\sigma}^2} \tag{13}$$

$$AIC = -2 * \ln(L) + 2K \tag{14}$$

$$BIC = -K * ln(L) + Kln(n) \tag{15}$$

where y_i represents the observed value for the *i-th* analytic tree; $\hat{y_i}$ is the predicted value of *i-th* observed value; *n* is the number of trees, $\overline{y}$ is the mean value for the observed values, $\hat{\sigma_b}^2$ is random intercept variance,$\hat{\sigma}^2$ is residual variance, *L* is the value of log-likelihood, *K* is the number of parameters in the model.

2.6 Uncertainty analysis

The total uncertainty of forest stand mean heights at pixel level is divided into three independent terms, each terms reported as a percentage of relative uncertainty, following Saatchi et al. (2011):

Measurement error ($\varepsilon_{measurement}$) is associated with the accuracy of individual tree segmentation from close-range LiDAR data. This study employs (1−F1 score) value as a measure of the percentage of relative uncertainty. The overall F1 score value averaged across all the testing plots was 0.90 with a corresponding measurement uncertainty of 10% (Li et al. 2012).

Product error ($\varepsilon_{product}$) refers to errors in estimating forest age (Cheng et al. 2024a) from forest structure attributes maps. It was estimated from the relations developed from calibration plots. The relative uncertainty of forest age for each pixel is calculated using Equation 16, and then the maximum of mean relative error of forest age is calculated using Equation 17 (Supplementary Note S1).

$$\varepsilon_i = \frac{RMSE}{\hat{y_i}} * 100\% \tag{16}$$

$$\bar{\varepsilon}_{max} = \frac{RMSE}{\overline{y}} \times 100\% \tag{17}$$

where *RMSE* is the root mean squared error of the validation set for the forest age product, $\hat{y_i}$ represents the predicted value of the *i-th* observed value.

Prediction error ($\varepsilon_{prediction}$) includes both the sampling error associated with the representativeness of the training data relative to the actual spatial distribution of stand height, as well as the model predictions. The relative uncertainty for each pixel is calculated as:

$$\varepsilon_{prediction} = \frac{RMSE_h}{\hat{h}_i} * 100\% \tag{18}$$

where $RMSE_h$ is the root mean squared error of the validation set, $\hat{h}_i$ represents the predicted stand height value of the *i-th* observed stand height value.

Finally, we propagated the errors through the entire process by assuming all errors were independent and random. The uncertainty in estimating stand mean height (ε_h) was quantified using:

$$\varepsilon_{h_i} = \sqrt{\varepsilon_{measurement}^2 + \varepsilon_{product}^2 + \varepsilon_{prediction}^2} \tag{19}$$

To calculate the national-level uncertainty, we sum the errors from all pixels using:

$$\varepsilon_{national} = \frac{\sqrt{\sum_{i=1}^{N}(\hat{h}_i \varepsilon_{h_i})^2}}{\sum_{i=1}^{N} \hat{h}_i} \tag{20}$$

where *N* is the number of pixels within the national boundary, and $\hat{h}_i$ and ε_{h_i} are the stand height and its relative uncertainty at pixel *i*, respectively.

3 Results

3.1 UAV LiDAR-derived arithmetic mean height (h_a) and weighted mean height (h_w) across China

The UAV LiDAR-derived h_a and h_w varied across seven vegetation divisions (excluding Qinghai-Tibet Plateau alpine vegetation), However, as illustrated in Figure.4, the rankings of h_a and h_w remained consistent across these vegetation divisions. The tallest LiDAR-derived h_a and h_w were recorded in the tropical monsoon forest-rainforest, measuring 68.49 m and 69.67 m, respectively. In contrast, the highest average LiDAR-derived h_a and h_w were observed in the temperate desert, with values of 30.55 ± 6,94 m and 37.28 ± 5.58 m, respectively (Fig. 4). The range of UAV LiDAR-derived h_a and h_w distribution was widest in the tropical monsoon forest-rainforest, with standard deviations of 8.00 m and 9.15m, respectively (Fig. 4). While the lowest standard deviations of h_a and h_w were recorded in the cold temperate needleleaf forest, with values of 2.17m and 1.94 m, respectively (Fig. 4). These UAV LiDAR-derived h_a and h_w provided a concrete foundation for training and validating the tree-based approach for mapping wall-to-wall h_a and h_w of China's forest.
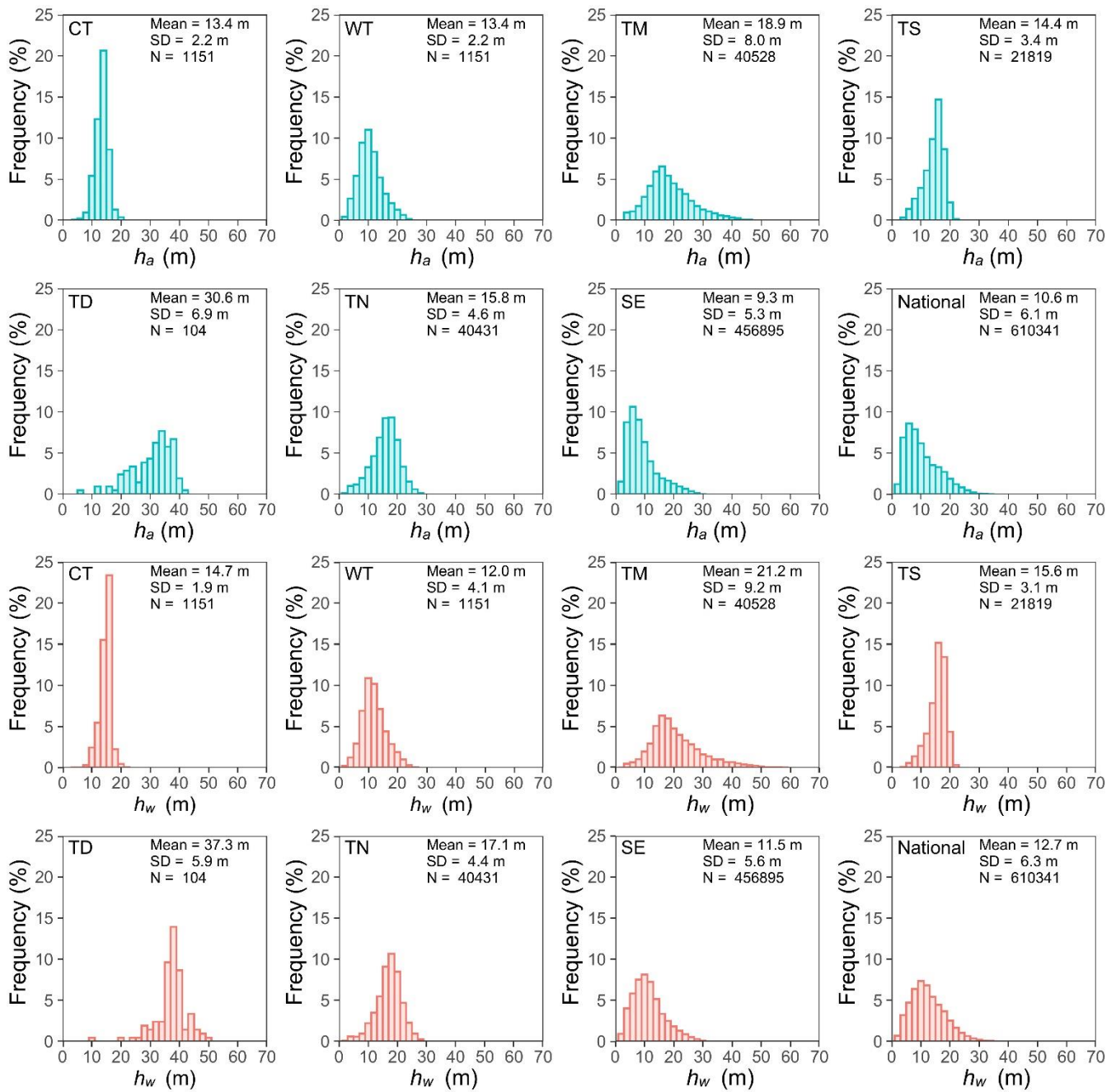
Figure 4: Histograms of UAV LiDAR-derived h_a and h_w across vegetation zone and the overall dataset. Mean and SD represent the mean and standard deviation of UAV LiDAR-derived h_a and h_w, with N represents the number of training sample plots (size =30 × 30 m). CT, TN, TS, TD, WT, SE, and TM represent the vegetation divisions of cold temperate needleleaf forest, temperate needleleaf-broadleaf mixed forest, temperate steppe, temperate desert, warm temperate deciduous-broadleaf forest, subtropical evergreen broadleaf forest, and tropical monsoon forest-rainforest, respectively.

305

310

3.2 Prediction accuracy of MLME model

Based on the construction and optimization process of ML model (see Supplementary Table S6 and S7), the MLME models simultaneously account for the interaction between covariates (the predicted h_a and h_w from the ML) and the grouping variable (eight vegetation divisions). These models, as shown in Table 3 and Table 4, reveal different predictions of h_a and h_w across vegetation divisions. This study suggests that discrepancies in estimating h_a and h_w across China primarily stem from variations in vegetation divisions, as evidenced by ICC values of 0.581 and 0.693 for h_a and h_w, respectively (Table 4). These values indicated that approximately 58.1% and 69.3% of the total variance are attributable to variations between different vegetation divisions for estimating h_a and h_w, respectively (Table 4).

Table 4. Parameter estimates and fitting statistics of MLME models for vegetation divisions.

	Vegetation division	h_a		h_w	
		b	β	b	β
Parameter estimates	CT	0.182	0.989	-0.249	1.016
	WT	-0.108	1.007	-0.249	1.018
	TM	0.133	0.992	-0.249	1.011
	TS	0.111	0.993	-0.249	1.015
	TD	0.56	0.964	-0.249	1.016
	TN	0.284	0.982	-0.249	1.016
	SE	-0.042	1.003	-0.249	1.021
Fitting statistics	ICC	0.581		0.693	
	AIC	962107		1008650	
	BIC	962168		1008711	
	logLik	-481048		-504319	
	Pr (>Chisq)	3.37E-05***		9.29 E-06***	

Notes: h_a is arithmetic mean height; h_w is weighted mean height; CT is cold temperate needleleaf forest, TN is temperate needleleaf-broadleaf mixed forest, TM is tropical monsoon forest-rainforest, TS is temperate steppe, TD is temperate desert, WT is warm temperate deciduous-broadleaf forest, SE is subtropical evergreen broadleaf forest.

Our results demonstrated high accuracy in estimating h_a and h_w across China's forests, with $R^2 > 0.82$, RMSE < 2.6 m and MAE < 1.9 m for h_a and $R^2 > 0.78$, RMSE < 2.9 m and MAE < 2.1 m for h_w (Table 5 and Fig. 5). It can be seen that the accuracy of h_a consistently surpasses that of h_w, regardless of whether ML or MLME methods were employed. As displayed in Table 5 and Fig. 5, MLME models, which integrated vegetation divisions as variables, showed slightly superior performance in estimating h_a and h_w compared to ML models, once again highlighting the impact of incorporating vegetation divisions on

the estimation results. Additionally, incorporating vegetation divisions improved the accuracy of h_w estimation slightly when

330   compared to that of h_a, This may be due to the stronger influence of vegetation divisions on h_w (ICC=0.693) (Table 4 and 5). Fig. 5 provides comparisons of estimated h_a and h_w against observed LiDAR validation data based on MLME. Excellent consistency can be found between estimated and validation results. High correlations are presented in the h_a MLME model (r=0.906), as well as h_w MLME model (r=0.889). Specifically, the h_a tended to be slightly overestimated for lower measured mean height, while no biased estimation was observed for h_w.

335   **Table 5** Comparative prediction accuracy of h_a and h_w models with ML and MLME.

Model	Method	R²	RMSE	rRMSE	MAE
h_a	ML	0.8209	2.5744	24.1707%	1.8581
	MLME	0.8209	2.5741	24.1679%	1.8567
h_w	ML	0.7892	2.8876	22.7418%	2.0940
	MLME	0.7895	2.8859	22.7284%	2.0888

Notes: h_a is arithmetic mean height; h_w is weighted mean height
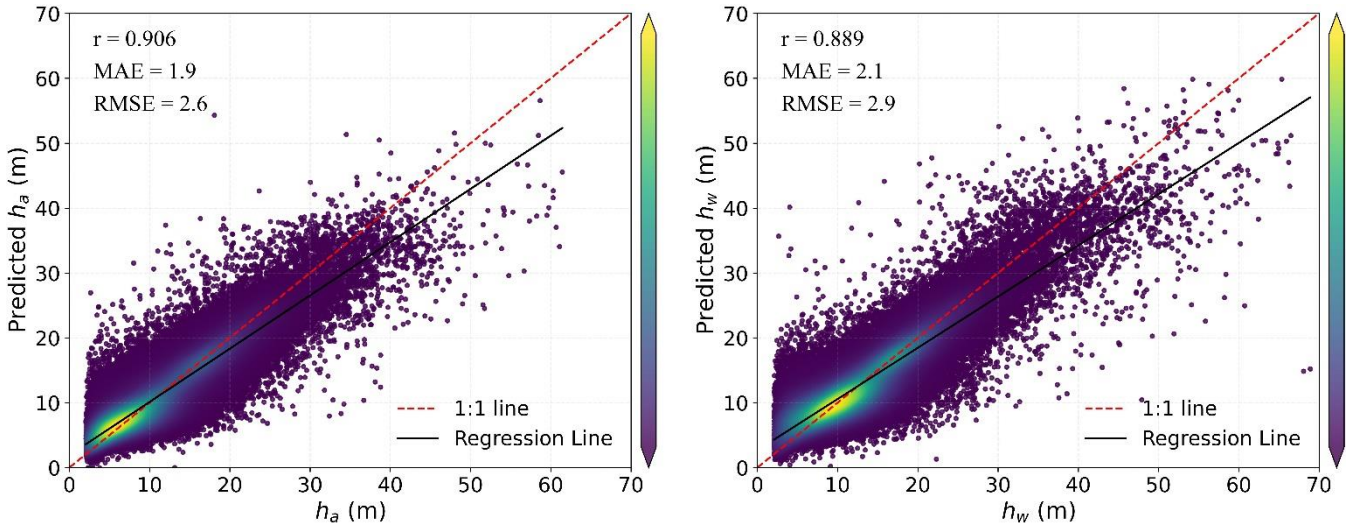
Figure 5: Accuracy assessment of the MLME-derived h_a and h_w when compared with LiDAR validation data.

3.3 Wall-to-wall arithmetic mean height (h_a) and weighted mean height (h_w) of China

340   We applied MLME models to map h_a and h_w at a 30 m resolution across China's forests, as shown in Fig. 6 and Fig. 7, respectively. Overall, the mean value of h_w was 13.3 ± 3.3 m (mean value ± SD) for pixels, which is higher than that of h_a (11.3 ± 2.9 m) per pixels. Geographically, our h_a and h_w maps exhibited similar patterns, with forests in the southwestern (h_a = 12.05 ± 3.27 m, h_w = 14.13 ± 3.85 m), northeastern (h_a = 12.05 ± 3.20 m, h_w = 14.74 ± 3.39 m), and southeastern (h_a =10.98 ± 2.67 m, h_w = 12.67 ± 2.60 m) part of China being relatively taller than those in the southern (h_a = 10.69 ± 2.39 m,

345   h_w = 12.56 ± 2.39 m), northern (h_a = 10.28 ± 2.44 m, h_w = 11.80 ±2.43 m) and northwestern (h_a = 10.63 ± 2.53 m, h_w =

12.59 ± 2.87 m) regions (Figs. 6 and 7). Despite considerable variations in h_a and h_w among forests in different provinces (Fig. 8), a consistent trend indicated that h_a was generally lower than h_w across all provinces, except for Tianjin ($h_a = 8.78 \pm 1.64$ m VS. $h_w = 8.34 \pm 1.64$ m) (Fig. 8). Notably, Jilin exhibited the highest h_a value (13.41 ± 2.92 m), closely followed by Tibet (13.40 ± 3.60 m), Anhui (12.96 ± 2.65 m), Xinjiang (12.39 ± 4.01 m), and Sichuan (12.21 ± 3.02 m). Conversely,

350   Shanghai recorded the highest h_w value (17.17 ± 2.02 m), with Jilin (17.12 ± 2.87 m), Xinjiang (16.93 ± 2.54 m), Tibet (16.21 ± 4.73 m), and Yunnan (15.03 ± 4.02 m) trailing closely behind. Tibet, Xinjiang and Yunnan showed greater variability in both h_a and h_w than in other provinces.
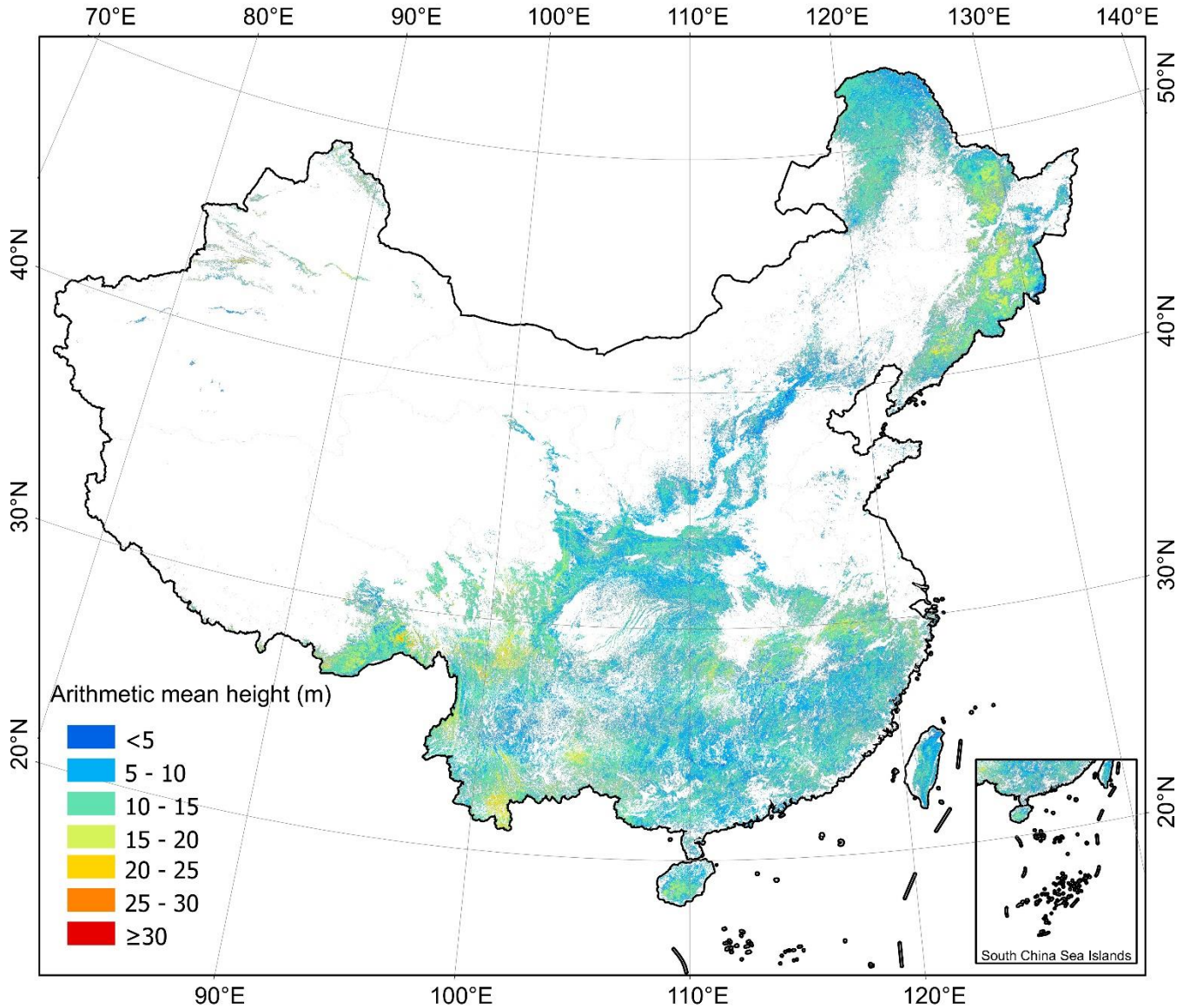
Figure 6: The forest arithmetic mean height (h_a) of China derived from the tree-based approach at 30 m resolution for 2020.
355   **Publisher's remark: please note that the above figure contains disputed territories.**

Figure 7: The forest weighted mean height (h_w) of China derived from tree-based approach at 30 m resolution for 2020. Publisher's remark: please note that the above figure contains disputed territories.
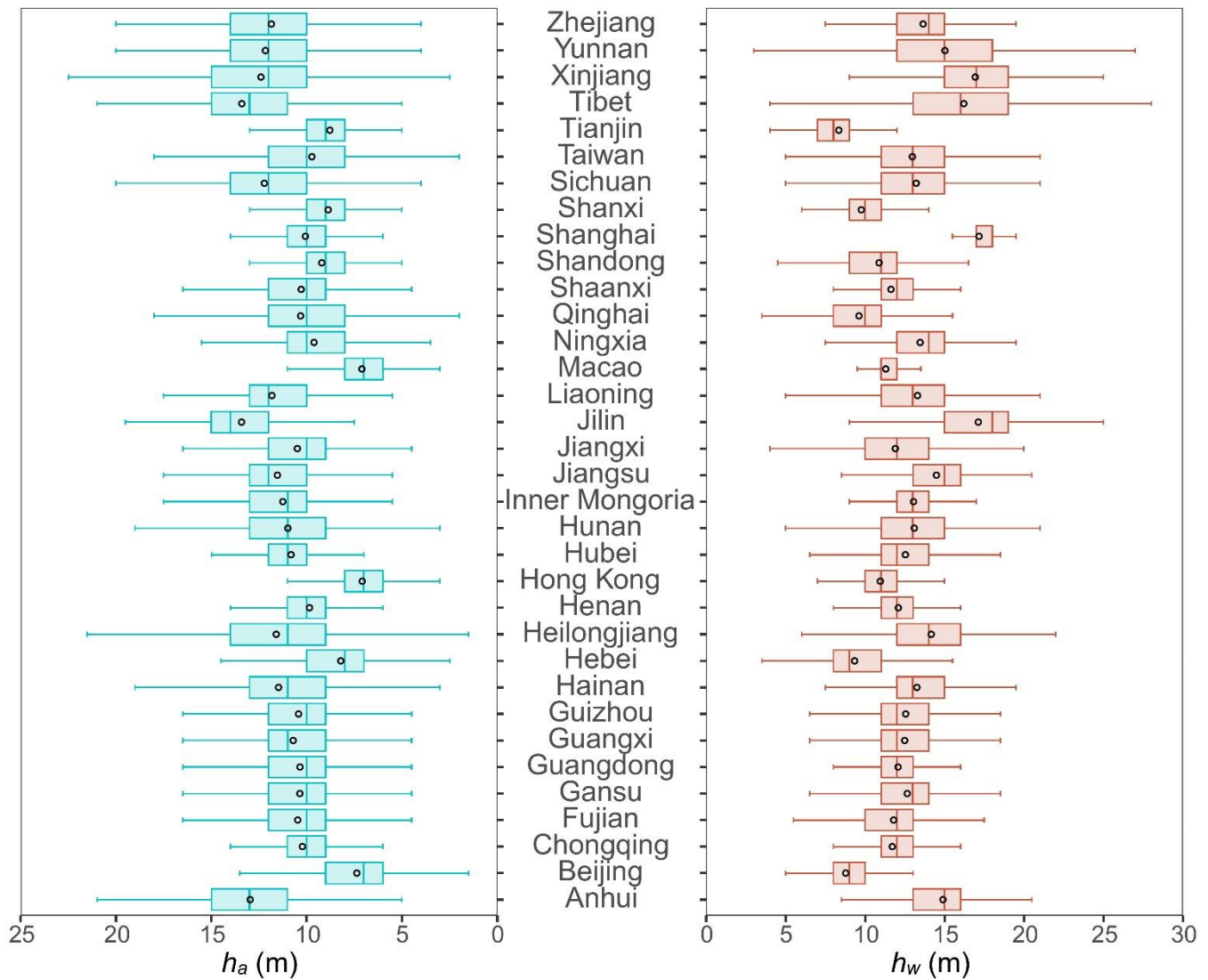
360 **Figure 8: Province-level analysis of h_a and h_w estimations derived from tree-based approach. The black circle is the mean value, the solid line in box is median value for each province.**

The estimations for h_a and h_w conformed to a normal distribution across eight vegetation divisions in China, with there are some notable differences between the two as shown in Fig. 9. The highest recorded values for h_a and h_w values were 94 m and 96 m, respectively, observed in subtropical evergreen broadleaf forest. For h_a, the temperate needleleaf-broadleaf mixed

365 forest exhibited the tallest forest height (median = 13 m, mean = 13.03 m), followed by tropical monsoon forest-rainforest (median = 13 m, mean = 12.95 m), Qinghai-Tibet Plateau alpine vegetation (median = 12 m, mean = 12.38 m), temperate desert (median = 11 m, mean = 11.83 m), subtropical evergreen broadleaf forest (median = 11 m, mean = 11.14 m), temperate steppe (median = 11 m, mean = 10.78 m), cold temperate needleleaf forest (median = 11 m, mean = 10.75 m) and warm

temperate deciduous-broadleaf forest (median = 9 m, mean = 9.34 m). For h_w, tropical monsoon forest-rainforest had the
370   tallest forest height (median = 16 m, mean = 16.41 m), followed by temperate needleleaf-broadleaf mixed forest (median = 16
m, mean = 15.96 m), temperate desert (median = 16 m, mean = 15.44 m), cold temperate needleleaf forest (median = 13 m,
mean = 12.89 m), subtropical evergreen broadleaf forest (median = 12 m, mean = 12.84 m), temperate steppe (median = 13 m,
mean = 12.80 m), Qinghai-Tibet Plateau alpine vegetation (median = 12 m, mean = 12.34 m) and warm temperate deciduous-
broadleaf forest (median = 11 m, mean = 10.77 m). Compared to the ranges of h_a distributions in different vegetation divisions,
375   the ranges of h_w distributions were wider as illustrated in Fig. 9. Specifically, the vegetation divisions with the greatest
variations, the ranges of both h_a and h_w distributions were temperate desert (standard deviation = 4.09 m and 4.55 m of h_a
and h_w, respectively), tropical monsoon forest-rainforest (standard deviation = 3.71 m and 4.39 m of h_a and h_w, respectively),
and temperate needleleaf-broadleaf mixed forest (standard deviation = 3.10 m and 3.27 m of h_a and h_w, respectively).
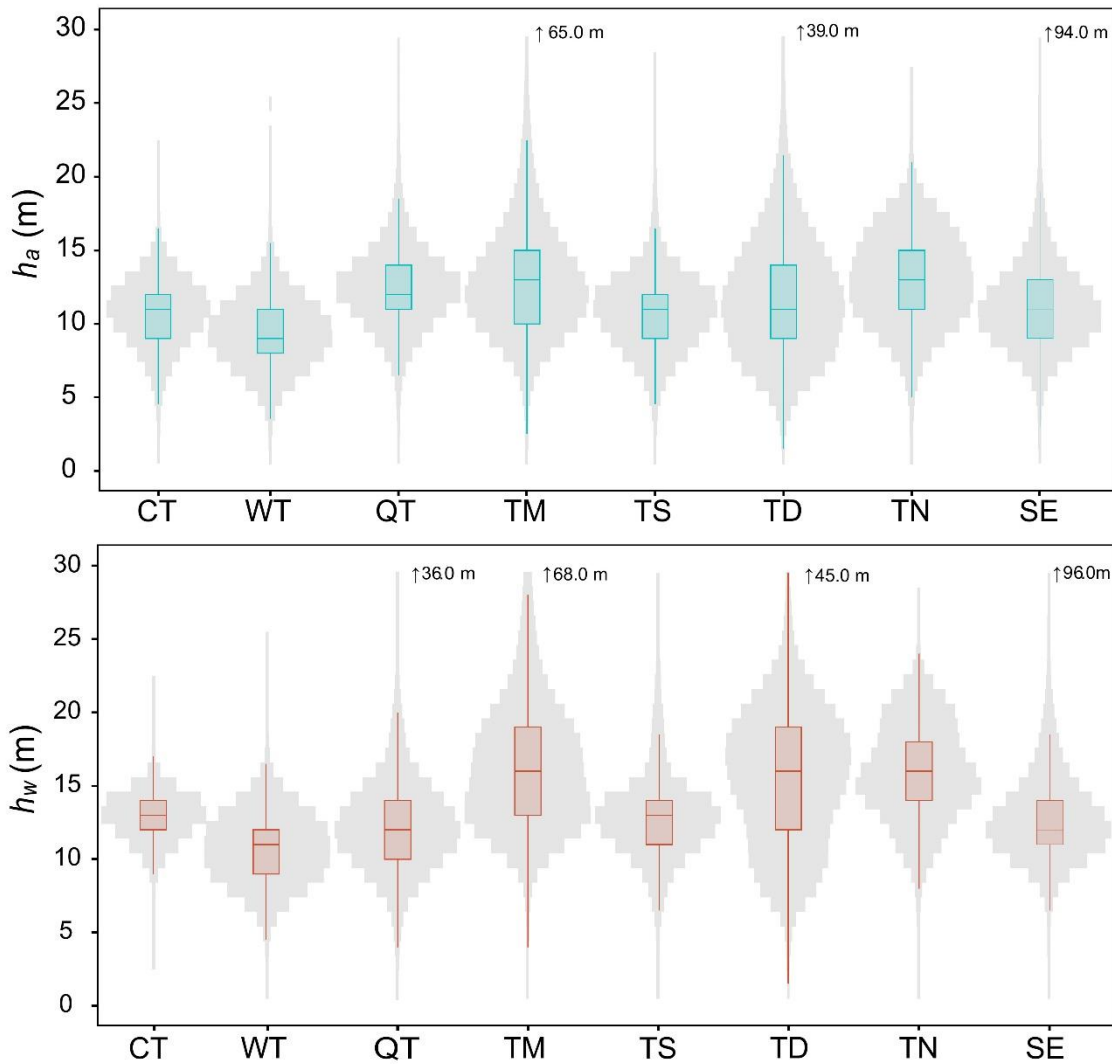
Figure 9: Vegetation divisions-level analysis of the tree-based approach-derived h_a and h_w estimations. CT, TN, TS, TD, WT, QT, SE, and TM represent the vegetation divisions of cold temperate needleleaf forest, temperate needleleaf-broadleaf mixed forest, temperate steppe, temperate desert, warm temperate deciduous-broadleaf forest, Qinghai-Tibet Plateau alpine vegetation, subtropical evergreen broadleaf forest, and tropical monsoon forest-rainforest, respectively. The solid line in each box is median value.

3.4 Uncertainty analysis

The uncertainties of h_a (Fig. 10) and h_w (Fig. 11) at the 30 m pixel level were quantified by integrating measurement error, product error, and prediction error of h_a and h_w maps. The overall uncertainty in mapping h_a and h_w at the pixel scale, averaged over all vegetation divisions, was estimated to be 23% and 21%, respectively (Fig. 10 and Fig. 11). However, these uncertainties were not uniformly distributed across China. The uncertainty for h_a ranged from 16% to 56%, while for h_w, it ranged from 16% to 59%. These variations depended on regional differences in forests, the quality of remote sensing imagery, and the sampling size and distribution of available field and LiDAR data. We further assessed the uncertainty around h_a and h_w estimates at national and regional scales by errors propagation. As the sample area increased, the relative errors decreased. The national estimations were found to be constrained to within 1% for h_a (4.30×10^{-4} %) and h_w (4.12×10^{-4} %).
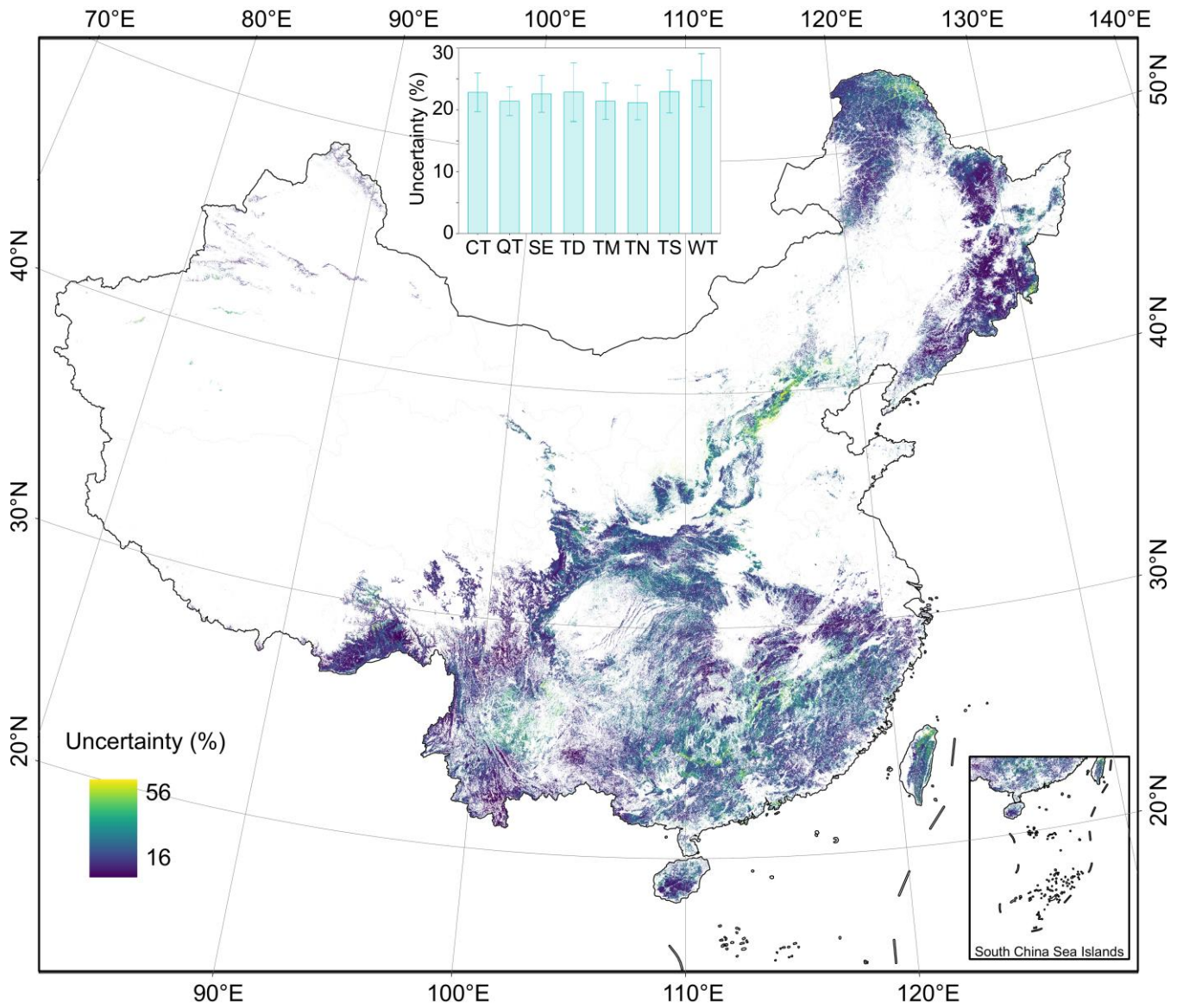
Figure 10: Uncertainty analysis in the spatial distribution of forest arithmetic mean height (h_a) in each pixel. Publisher's remark: please note that the above figure contains disputed territories.
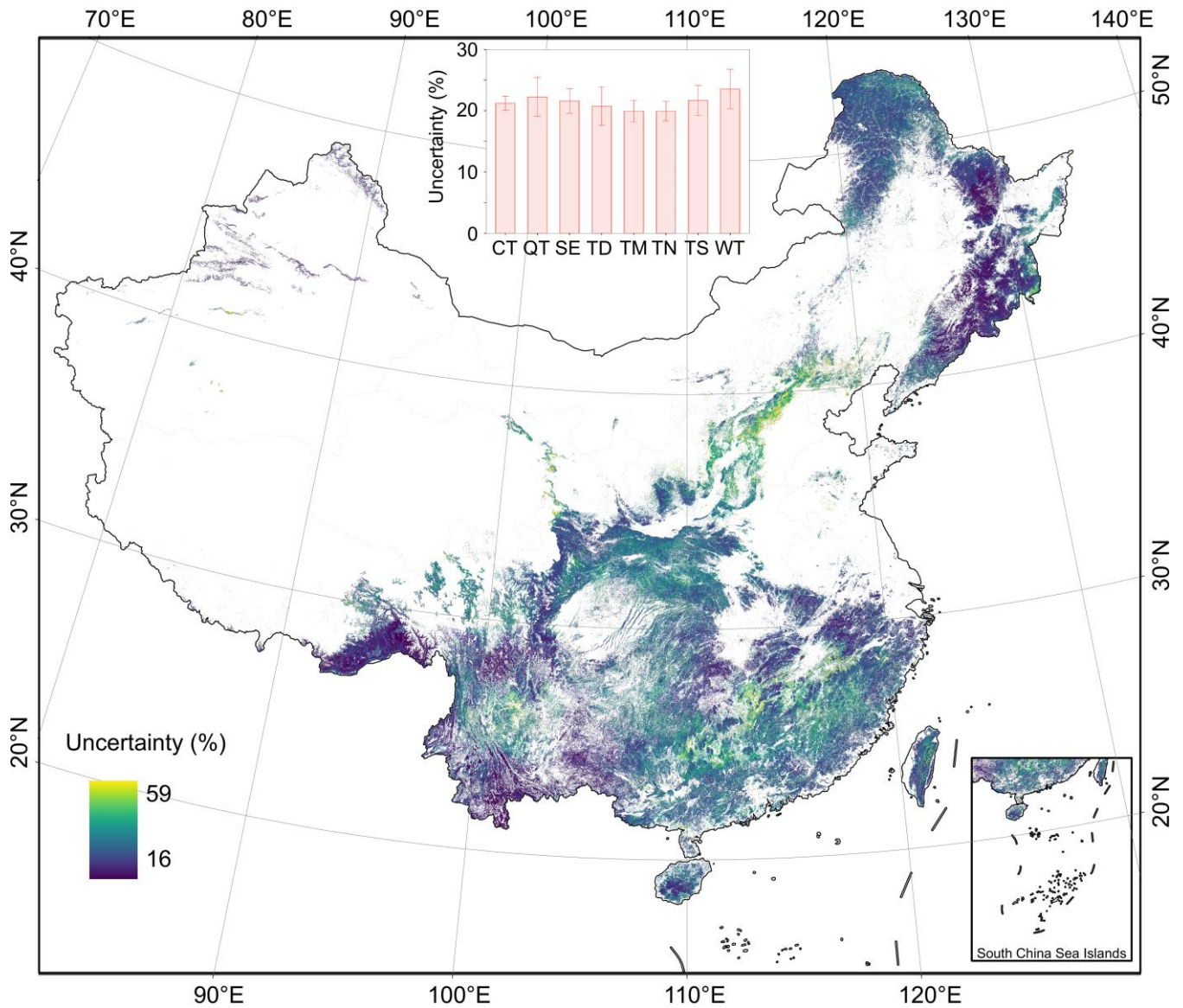
Figure 11: Uncertainty analysis in the spatial distribution of forest weighted mean height (h_w) in each pixel. Publisher's remark: please note that the above figure contains disputed territories.

4 Discussion

The national scale, continuous maps of arithmetic mean height (h_a) and weighted mean height (h_w) across China address the challenges of accurately estimating forest stand mean height using a tree-based approach. These maps provide critical datasets for forest sustainable management in China, including climate change mitigation (e.g., terrestrial carbon estimation) (Duncanson et al. 2022; Migliavacca et al. 2021), forest ecosystem assessment (Davies et al. 2017; Jucker et al. 2018; Li et al.

405 2020), and forest inventory practices (Fang et al. 2006; Fang et al. 2001; Travers-Smith et al. 2024; Xu et al. 2019). By leveraging high-point density, and high-precision close-range LiDAR data, spatially continuous maps that comply with the definitions of h_a and h_w in forestry were generated. Validation results indicate that our method has a high accuracy (Figs. 5 and 12), demonstrating the potential for widespread application of tree-based forest stand mean height estimation at large-scale. Furthermore, our findings suggest that close-range LiDAR technology can enhance traditional forestry surveys by

410 enabling rapid, accurate, large-scale, and cost-effective assessments.

Regarding forest stand mean height estimations (h_a and h_w), distinctive methods and definitions of tree height from the commonly used CHM are employed in this study. Despite these differences, previous studies indicate that there was a strong correlation between forest stand mean height and the CHM-derived height metrics from LiDAR point clouds. Finer scale analysis demonstrated that the 50%, 75%, 80%, 90%, and 95% percentile heights in the CHM model can serve as the optimal

415 variables for linear regression prediction of Lorey's weighted height across different studies (Li et al. 2022; Liu et al. 2018; Pang et al. 2008). Conversely, for predicting arithmetic mean height, different optimal variables might be employed, including the 30%, 60%, and 70% percentile heights (Jensen and Mathews 2016; Li et al. 2022). The above-mentioned differences resulting from variations in geographic regions and tree species highlight the challenges in indirectly estimating h_a and h_w using the CHM (Yin et al. 2024). Spaceborne LiDAR and multi-source remote sensing data have been widely used for

420 estimating forest canopy height on national/global scale through area-based approaches (Coops et al. 2021; Liu et al. 2022; Travers-Smith et al. 2024), including the 98% percentile height (Lang et al. 2023; Liu et al. 2022), 95% percentile height (Potapov et al. 2021), 100% percentile height (Ni et al. 2015; Simard et al. 2011), and 90% percentile height canopy height products. However, these results are more align with the maximum tree height which may be numerically closer to the forest dominant/top height (Li et al. 2023), rather than the forestry definitions of forest stand mean height (Laar and Akça 2007;

425 Masaka et al. 2013). In forestry, the dominant tree height is widely recognized as a key factor in explaining forest site productivity (Vanclay 1992; Vatandaslar et al. 2023; Woods et al. 2011), while stand mean heights are crucial for calculating forest volume and carbon storage capacity (Xu et al. 2019). As the demand for accurate tree height estimation grows, our study aligns with forestry definitions and needs. Taking advantages of extensive high-precision UAV LiDAR data, we mapped the national-scale forest h_a and h_w data products for China. Among them, h_a can efficiently and accurately assesses the stand

430 mean height in even-aged stands (e.g., planted forest), while h_w is a valuable parameter for representing the mean height in uneven-aged forest stands (e.g., natural forest). Our maps underscore the importance of using appropriate tree height definitions and methodologies tailored to meet the specific requirements of forestry management and ecological research.

A significant challenge of using a tree-based approach to calculated Lorey's weighted height from UAV LiDAR data lies in the difficulty of obtaining DBH information. Consequently, the traditional Lorey's weighted height calculation method is not

435 feasible in this study. To address this problem, the regression height of the quadratic mean diameter method, which estimate stand mean height by corresponding to the tree height with average DBH on the height-diameter curve, served as a simplified alternative (Laar and Akça 2007; Lou et al. 2016). Therefore, following Næsset (1997), this study uses accurate tree height measurements obtained from UAV LiDAR, treating tree height itself as the weight to calculate the weighted mean height (h_w)

in this study. This method mitigates the limitations of applying Lorey's weighted height without DBH, yielding results that are highly consistent with those obtained using DBH-based ones (Fig. 3). However, as highlighted in Fig. 3, our weighting method shows a tendency to overestimate tree heights. We explored this issue through both theoretical derivation and empirical validation to offer a more comprehensive interpretation (detailed in Supplementary Note S2). Our analysis reveals that the overestimation of h_w occurs mainly when the numerical value of DBH (measured in cm) consistently exceeds that of tree height (measured in meters), a rare and extreme scenario. Additionally, limitations in our validation data, such as its small sample size and uneven distribution, may have contributed to this discrepancy. Nonetheless, the h_w calculation method used in this study is easy to apply to large-scale forest surveys, significantly reducing the input of labor, time, and costs.

Another challenge arises from the regional variations that affect tree height in China, due to the extensive distribution of China's forest. In this study, a variety of variables related to forest growth were considered in a comprehensive way to address this issue (detailed in section 2.3), thereby enhancing the model's explanatory force and improving the accuracy of h_a and h_w estimations. Additionally, forest stand mean height is significantly influenced by tree species (Laar and Akça 2007). However, obtaining accurate tree species information through large-scale and remote sensing-based methods is a challenging (Ørka et al. 2009). For example, Wu and Shi (2023) considered the distinct nature of forests in different ecological zones in China, as a feasible method in the absence of known tree species, to improve the accuracy of forest canopy height estimation through building ecological zone-based models. Similarly, to avoid the potential boundary effects introduced by multiple specific models, we applied MLME model to capture and differentiate forest types in vegetation divisions across China. It was revealed that 58.1% and 69.3% of the total variances of h_a and h_w were due to variations of vegetation divisions (Table 4). This indicates significant ecological differences between the vegetation divisions, leading to differences in h_a and h_w. Combining the results from Table 5, the MLME method showed a slight performance improvement over ML method in both h_a and h_w. Additionally, the improvement in h_w exceeds that in h_a, possibly due to its higher ICC as shown in Table 4, which further highlights that h_w is more sensitive to uneven-aged forest stands.
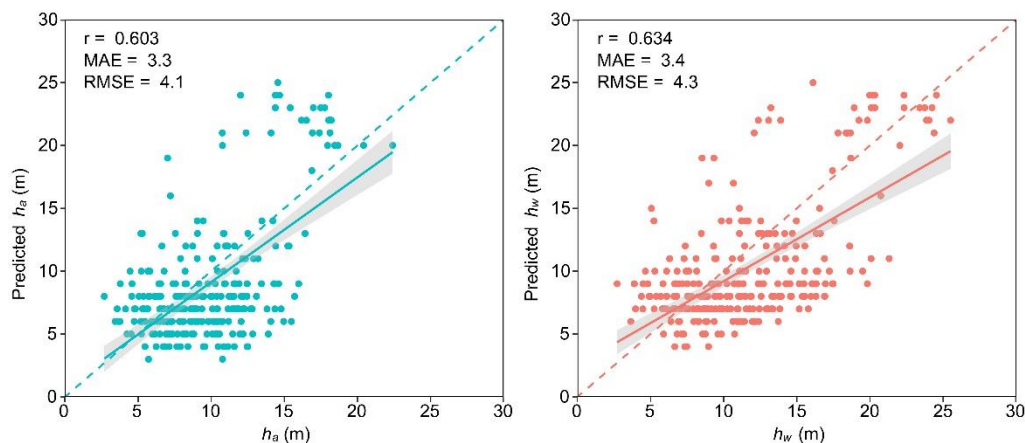
Figure 12: Accuracy assessment of forest mean heights (h_a and h_w) compared with filed measurements.

The validation results of both h_a and h_w estimations based on a tree-based approach, compared to the field-measured forest stand mean height, show an overestimation for plots with higher tree heights and a slight underestimation for plots with lower tree heights (Fig. 12). The values of r and RMSE for h_a and h_w indicate that h_a and h_w, when validated through LiDAR data, exhibit better performance (Figs. 5 and 12). Two reasons are likely to influence the accuracy assessment of h_a and h_w in this study. First, there may be certain errors in both field-based and LiDAR-based tree height measurements may have contributed. Variations of researchers and measurement tools, coupled with canopy occlusion can affect the accurate measurements of tree heights, particularly for the tall trees in field (Jurjević et al. 2020; Wang et al. 2019a). In this study, h_a and h_w estimations are influenced by accurate segmentation of individual trees based on LiDAR data. However, the accuracy of LiDAR-based individual tree segmentation is also affected by canopy occlusion (Huo et al. 2022; Li et al. 2012), especially the omission of low trees obscured by the canopy. This omission of trees with lower heights may increase the influence of the taller trees in h_w weighted by tree height, leading to overestimated results (Laar and Akça 2007; Lefsky 2010)(Fig. 12). Second, the lack of temporal consistency between LiDAR data and field measurements may be another reason. In this study, the LiDAR data were collected from 2015 to 2023, while the field measurements were conducted from 2019 to 2023 (Yang et al. 2023). The relatively long-time span may witness significant tree growth, particularly in young forests (Tang et al. 2014). Therefore, this temporal inconsistency may have impacted the estimation and validation of h_a and h_w. Specifically, it could cause an underestimation of tree heights below 10 m as shown in Figure 12.

Overall, despite the novelty of the data, maps of forest mean stand height, and topic in this study are new, there are still several limitations of the study in terms of close-range LiDAR data and algorithms of LiDAR process. First, as demonstrated in Figure 2, close-range LiDAR data are spatially unevenly distributed across China. While over 1117 km^2 of close-range LiDAR data were used, the gaps in data coverage over Qinghai-Tibet Plateau alpine vegetation divisions and uneven distribution in northwestern and southeastern China may influence the mapping accuracy. Enhancing data acquisition and establishing sharing mechanisms for LiDAR data might be key and feasible solutions to address this issue. Second, as shown in Table 1, training and validation data were sourced a nine-year span and collected using various LiDAR sensors. As of 2015, the application of LiDAR has not been widely adopted in forest remote sensing research in China. Considering the cost and the difficulty of data collection, it was challenging to collect extensive, high-point density and accurate data across China within a short timeframe. Consequently, multiple types of LiDAR sensors were employed over nine years to meet the requirements of data quality. Pre-processing and calibration were conducted to minimize the errors result from variations in LiDAR sensors (Guo et al. 2017; Hu et al. 2021; Zhao et al. 2022). While realizing potential errors associated with tree growth, there is no better alternative data available to achieve this tree-based approach to forest stand mean height mapping. Third, the accuracy of the individual tree segmentation algorithm based on UAV LiDAR data may be another limitation in this study. Accurate segmentation of individual trees is crucial for forest stand mean height mapping through a tree-based approach. Challenges such as omission and inclusion errors yield throughout individualizing trees in complex stands affect the accurate attribute measurements regarding individual trees, despite visual inspections. The accuracy of individual tree segmentation has also been included in

the uncertainty analysis, as shown in Figures. 10 and 11. The development of individual tree segmentation algorithm and fusion of multi-LiDAR platforms are expected in the future work to enhance individual tree segmentation accuracy.

5 Data availability

Data described in this manuscript can be accessed at the repository: https://doi.org/10.5281/zenodo.12697784 (Chen et al.,
500   2024).

6 Conclusion

We have developed a tree-based approach to create spatially continuous forest stand mean height maps across China through integrating high-point density, high-precision close-range LiDAR data and multisource remote sensing data. The accuracy analysis of h_a and h_w demonstrates the feasibility of the proposed method. A practical framework for forestry investigation
505   based on close-range LiDAR was proposed. The mean values of h_w and h_a are 13.3 ± 3.3 m and 11.3 ± 2.9 m on pixel level, respectively. Validation based on LiDAR and field sample data shows that the RMSE values, range from 2.6 to 4.1 m for h_a and 2.9 to 4.3 m for h_w, respectively, indicating that our approach outperforms existing forest canopy height maps derived from area-based approaches. Hopefully, our methods and maps will serve as a foundation for estimating carbon storage, monitoring changes in forest structure, managing forest inventory, and assessing wildlife habitat availability.

510   **Author contributions**

Y.C., H.Y. and Q.G. designed the study, Y.C. and H.Y. developed the MLME method, Z.Y., Q.Y., W.L., G.H., Y.R., K.C., T.X., M.C., D.L., Z.Q., J.X., Y.Z., and G.X. collected lidar data and provided the filed measurements, all of them processed the lidar data used in this study, Y.C. generated the forest stand mean height products of China and performed the accuracy assessment, H.Y. and Y.C. wrote the original manuscript, and all authors participated in the process of manuscript revisions.

515   **Competing interests**

The authors declare that they have no conflict of interest.

Disclaimer

Publisher's note: Copernicus Publications remains neutral with regard to jurisdictional claims made in the text. published maps, institutional affiliations, or any other geographical representation in this paper. While Copernicus Publications makes every

520 effort to include appropriate place names, the final responsibility lies with the authors. Regarding the maps used in this paper, please note that Figs,1, 2, 6, 7, 10 and 11 contain disputed territories.

Acknowledgements

We would like to thank all the scientists, engineers, and students who participated in the field observations, instrument maintenance, and data processing. We highly appreciate the valuable and constructive comments on the paper provided by

525 Yanjun Su of Institute of Botany CAS.

Financial support

This work was supported by the National Key Research and Development Program [No.2022YFF1300203], and the National Natural Science Foundation of China [grant number 42371329 and 32301285].

References

530 Akiba, T., Sano, S., Yanase, T., Ohta, T., and Koyama, M.: Optuna: A Next-generation Hyperparameter Optimization Framework, Proceedings of the 25th ACM SIGKDD International Conference on Knowledge Discovery & Data Mining, Anchorage, AK, USA, https://doi.org/10.1145/3292500.3330701, 2019.

Allard, D.: J.-P. Chilès, P. Delfiner: Geostatistics: Modeling Spatial Uncertainty, Mathematical Geosciences, 45, 377-380, 10.1007/s11004-012-9429-y, 2013.

535 Bouvier, M., Durrieu, S., Fournier, R. A., and Renaud, J.-P.: Generalizing predictive models of forest inventory attributes using an area-based approach with airborne LiDAR data, Remote Sens Environ, 156, 322-334, https://doi.org/10.1016/j.rse.2014.10.004, 2015.

Cheng, K., Chen, Y., Xiang, T., Yang, H., Liu, W., Ren, Y., Guan, H., Hu, T., Ma, Q., and Guo, Q.: A 2020 forest age map for China with 30 m resolution, Earth Syst. Sci. Data, 16, 803-819, https://doi.org/10.5194/essd-16-803-2024, 2024a.

540 Cheng, K., Yang, H., Guan, H., Ren, Y., Chen, Y., Chen, M., Yang, Z., Lin, D., Liu, W., Xu, J., Xu, G., Ma, K., and Guo, Q.: Unveiling China's natural and planted forest spatial–temporal dynamics from 1990 to 2020, ISPRS J Photogramm Remote Sens, 209, 37-50, https://doi.org/10.1016/j.isprsjprs.2024.01.024, 2024b.

Chen, Y., Yang, H., Yang, Z., Yang, Q., Liu, W., Huang, G., Ren, Y., Cheng, K., Xiang, T., Chen, M., Lin, D., Qi, Z., Xu, J., Zhang, Y., Xu, G., & Guo, Q.: Enhancing High-Resolution Forest Stand Mean Height Mapping in China through an Individual

545 Tree-Based Approach with Close-Range LiDAR Data (1.0) [Data set]. Zenodo. https://doi.org/10.5281/zenodo.12697784 ,2024.

Choi, S., McMaster, K. L., Kohli, N., Shanahan, E., Birinci, S., An, J., Duesenberg-Marshall, M., and Lembke, E. S.: Longitudinal effects of data-based instructional changes for students with intensive learning needs: A piecewise linear–linear mixed-effects modeling approach, J Educ Psychol, 116, 608-628, https://doi.org/10.1037/edu0000853, 2024.

550 Coops, N. C., Tompalski, P., Goodbody, T. R. H., Queinnec, M., Luther, J. E., Bolton, D. K., White, J. C., Wulder, M. A., van Lier, O. R., and Hermosilla, T.: Modelling lidar-derived estimates of forest attributes over space and time: A review of approaches and future trends, Remote Sens Environ, 260, 112477, https://doi.org/10.1016/j.rse.2021.112477, 2021.

Davies, A. B., Ancrenaz, M., Oram, F., and Asner, G. P.: Canopy structure drives orangutan habitat selection in disturbed Bornean forests, Proc Natl Acad Sci U S A, 114, 8307-8312, https://doi.org/10.1073/pnas.1706780114, 2017.

555 Demidenko, E.: Mixed models: theory and applications with R, 2nd Edition, John Wiley & Sons, ISBN 978-1-118-09157-9, 2013.

Donoghue, D. N. M. and Watt, P. J.: Using LiDAR to compare forest height estimates from IKONOS and Landsat ETM+ data in Sitka spruce plantation forests, Int J Remote Sens, 27, 2161-2175, https://doi.org/10.1080/01431160500396493, 2006.

Duncanson, L., Kellner, J. R., Armston, J., Dubayah, R., Minor, D. M., Hancock, S., Healey, S. P., Patterson, P. L., Saarela,
560 S., Marselis, S., Silva, C. E., Bruening, J., Goetz, S. J., Tang, H., Hofton, M., Blair, B., Luthcke, S., Fatoyinbo, L., Abernethy, K., Alonso, A., Andersen, H.-E., Aplin, P., Baker, T. R., Barbier, N., Bastin, J. F., Biber, P., Boeckx, P., Bogaert, J., Boschetti, L., Boucher, P. B., Boyd, D. S., Burslem, D. F. R. P., Calvo-Rodriguez, S., Chave, J., Chazdon, R. L., Clark, D. B., Clark, D. A., Cohen, W. B., Coomes, D. A., Corona, P., Cushman, K. C., Cutler, M. E. J., Dalling, J. W., Dalponte, M., Dash, J., de-Miguel, S., Deng, S., Ellis, P. W., Erasmus, B., Fekety, P. A., Fernandez-Landa, A., Ferraz, A., Fischer, R., Fisher, A. G.,
565 García-Abril, A., Gobakken, T., Hacker, J. M., Heurich, M., Hill, R. A., Hopkinson, C., Huang, H., Hubbell, S. P., Hudak, A. T., Huth, A., Imbach, B., Jeffery, K. J., Katoh, M., Kearsley, E., Kenfack, D., Kljun, N., Knapp, N., Král, K., Krůček, M., Labrière, N., Lewis, S. L., Longo, M., Lucas, R. M., Main, R., Manzanera, J. A., Martínez, R. V., Mathieu, R., Memiaghe, H., Meyer, V., Mendoza, A. M., Monerris, A., Montesano, P., Morsdorf, F., Næsset, E., Naidoo, L., Nilus, R., O'Brien, M., Orwig, D. A., Papathanassiou, K., Parker, G., Philipson, C., Phillips, O. L., Pisek, J., Poulsen, J. R., Pretzsch, H., Rüdiger, C., Saatchi,
570 S., Sanchez-Azofeifa, A., Sanchez-Lopez, N., Scholes, R., Silva, C. A., Simard, M., Skidmore, A., Stereńczak, K., Tanase, M., Torresan, C., Valbuena, R., Verbeeck, H., Vrska, T., Wessels, K., White, J. C., White, L. J. T., Zahabu, E., and Zgraggen, C.: Aboveground biomass density models for NASA's Global Ecosystem Dynamics Investigation (GEDI) lidar mission, Remote Sens Environ, 270, 112845, https://doi.org/10.1016/j.rse.2021.112845, 2022.

Fang, J., Chen, A., Peng, C., Zhao, S., and Ci, L.: Changes in Forest Biomass Carbon Storage in China Between 1949 and
575 1998, Science, 292, 2320-2322, https://doi.org/10.1126/science.1058629, 2001.

Fang, J., Brown, S., Tang, Y., Nabuurs, G.-J., Wang, X., and Shen, H.: Overestimated Biomass Carbon Pools of the Northern mid- and High Latitude Forests, Climatic Change, 74, 355-368, https://doi.org/10.1007/s10584-005-9028-8, 2006.

Fayad, I., Ciais, P., Schwartz, M., Wigneron, J.-P., Baghdadi, N., de Truchis, A., d'Aspremont, A., Frappart, F., Saatchi, S., Sean, E., Pellissier-Tanon, A., and Bazzi, H.: Hy-TeC: a hybrid vision transformer model for high-resolution and large-scale
580 mapping of canopy height, Remote Sens Environ, 302, 113945, https://doi.org/10.1016/j.rse.2023.113945, 2024.

Guo, Q., Su, Y., Hu, T., Guan, H., Jin, S., Zhang, J., Zhao, X., Xu, K., Wei, D., Kelly, M., and Coops, N. C.: Lidar Boosts 3D Ecological Observations and Modelings: A Review and Perspective, IEEE Geosci Remote Sens Mag, 9, 232-257, https://doi.org/10.1109/MGRS.2020.3032713, 2021.

Guo, Q., Su, Y., Hu, T., Zhao, X., Wu, F., Li, Y., Liu, J., Chen, L., Xu, G., Lin, G., Zheng, Y., Lin, Y., Mi, X., Fei, L., and

585 Wang, X.: An integrated UAV-borne lidar system for 3D habitat mapping in three forest ecosystems across China, Int J Remote Sens, 38, 2954-2972, https://doi.org/10.1080/01431161.2017.1285083, 2017.

Hall, R. J., Skakun, R. S., Arsenault, E. J., and Case, B. S.: Modeling forest stand structure attributes using Landsat ETM+ data: Application to mapping of aboveground biomass and stand volume, For Ecol Manage, 225, 378-390, https://doi.org/10.1016/j.foreco.2006.01.014, 2006.

590 Hu, J. and Szymczak, S.: A review on longitudinal data analysis with random forest, Brief Bioinform, 24, bbad002, https://doi.org/10.1093/bib/bbad002, 2023.

Hu, T., Sun, X., Su, Y., Guan, H., Sun, Q., Kelly, M., and Guo, Q.: Development and Performance Evaluation of a Very Low-Cost UAV-Lidar System for Forestry Applications, Remote Sensing, https://doi.org/10.3390/rs13010077, 2021.

Huang, H., Liu, C., Wang, X., Biging, G. S., Chen, Y., Yang, J., and Gong, P.: Mapping vegetation heights in China using

595 slope correction ICESat data, SRTM, MODIS-derived and climate data, ISPRS J Photogramm Remote Sens, 129, 189-199, https://doi.org/10.1016/j.isprsjprs.2017.04.020, 2017.

Huo, L., Lindberg, E., and Holmgren, J.: Towards low vegetation identification: A new method for tree crown segmentation from LiDAR data based on a symmetrical structure detection algorithm (SSD), Remote Sens Environ, 270, 112857, https://doi.org/10.1016/j.rse.2021.112857, 2022.

600 Jensen, J. L. R. and Mathews, A. J.: Assessment of Image-Based Point Cloud Products to Generate a Bare Earth Surface and Estimate Canopy Heights in a Woodland Ecosystem, Remote Sensing, https://doi.org/10.3390/rs8010050, 2016.

Jucker, T., Hardwick, S. R., Both, S., Elias, D. M. O., Ewers, R. M., Milodowski, D. T., Swinfield, T., and Coomes, D. A.: Canopy structure and topography jointly constrain the microclimate of human-modified tropical landscapes, Glob Chang Biol, 24, 5243-5258, https://doi.org/10.1111/gcb.14415, 2018.

605 Jurjević, L., Liang, X., Gašparović, M., and Balenović, I.: Is field-measured tree height as reliable as believed – Part II, A comparison study of tree height estimates from conventional field measurement and low-cost close-range remote sensing in a deciduous forest, ISPRS J Photogramm Remote Sens, 169, 227-241, https://doi.org/10.1016/j.isprsjprs.2020.09.014, 2020.

Kwong, I. H. Y. and Fung, T.: Tree height mapping and crown delineation using LiDAR, large format aerial photographs, and unmanned aerial vehicle photogrammetry in subtropical urban forest, Int J Remote Sens, 41, 5228-5256,

610 https://doi.org/10.1080/01431161.2020.1731002, 2020.

Laar, A. v. and Akça, A.: Measurement Of Stands, in: Forest Mensuration, edited by: Laar, A. v., and Akça, A., Springer Netherlands, Dordrecht, 95-147, https://doi.org/10.1007/978-1-4020-5991-9_5, 2007.

Lang, N., Jetz, W., Schindler, K., and Wegner, J. D.: A high-resolution canopy height model of the Earth, Nat Ecol Evol, 7, 1778-1789, https://doi.org/10.1038/s41559-023-02206-6, 2023.

615 Lefsky, M. A.: A global forest canopy height map from the Moderate Resolution Imaging Spectroradiometer and the Geoscience Laser Altimeter System, Geophys Res Lett, 37, https://doi.org/10.1029/2010GL043622, 2010.

Lefsky, M. A., Harding, D. J., Keller, M., Cohen, W. B., Carabajal, C. C., Del Bom Espirito-Santo, F., Hunter, M. O., and de Oliveira Jr, R.: Estimates of forest canopy height and aboveground biomass using ICESat, Geophys Res Lett, 32, https://doi.org/10.1029/2005GL023971, 2005.

620 Li, C., Chen, Z., Zhou, X., Zhou, M., and Li, Z.: Generalized models for subtropical forest inventory attribute estimations using a rule-based exhaustive combination approach with airborne LiDAR-derived metrics, GIsci Remote Sens, 60, 2194601, https://doi.org/10.1080/15481603.2023.2194601, 2023.

Li, M., Liu, Q., Feng, Y., and Li, Z.: Analysis of estimation models of plantation stand heights using UAV LiDAR, National Remote Sensing Bulletin, 26, 2665-2678, 10.11834/jrs.20210246 ,2022.

625 Li, W., Guo, Q., Jakubowski, M. K., and Kelly, M.: A new method for segmenting individual trees from the lidar point cloud, Photogramm Eng Remote Sensing, 78, 75-84, https://doi.org/10.14358/PERS.78.1.75, 2012.

Li, W., Niu, Z., Shang, R., Qin, Y., Wang, L., and Chen, H.: High-resolution mapping of forest canopy height using machine learning by coupling ICESat-2 LiDAR with Sentinel-1, Sentinel-2 and Landsat-8 data, Int J Appl Earth Obs Geoinf, 92, 102163, https://doi.org/10.1016/j.jag.2020.102163, 2020.

630 Liang, X., Kukko, A., Balenović, I., Saarinen, N., Junttila, S., Kankare, V., Holopainen, M., Mokroš, M., Surový, P., Kaartinen, H., Jurjević, L., Honkavaara, E., Näsi, R., Liu, J., Hollaus, M., Tian, J., Yu, X., Pan, J., Cai, S., Virtanen, J. P., Wang, Y., and Hyyppä, J.: Close-Range Remote Sensing of Forests: The state of the art, challenges, and opportunities for systems and data acquisitions, IEEE Geosci Remote Sens Mag, 10, 32-71, https://doi.org/10.1109/MGRS.2022.3168135, 2022.

Liu, H., Zhang, Z., and Cao, L.: Estimating forest stand characteristics in a coastal plain forest plantation based on vertical 635 structure profile parameters derived from ALS data, Journal of Remote Sensing, 22, 872-888, 10.11834/jrs.20187465,2018.

Liu, X., Su, Y., Hu, T., Yang, Q., Liu, B., Deng, Y., Tang, H., Tang, Z., Fang, J., and Guo, Q.: Neural network guided interpolation for mapping canopy height of China's forests by integrating GEDI and ICESat-2 data, Remote Sens Environ, 269, 112844, https://doi.org/10.1016/j.rse.2021.112844, 2022.

Lorey, T.: Die mittlere bestandeshöhe, J Allgemeine Forst-und jagdzeitung, 54, 149-155, 1878.

640 Lou, M., Zhang, H., Lei, X., Li, C., and Zang, H.: Spatial Autoregressive Models for Stand Top and Stand Mean Height Relationship in Mixed Quercus mongolica Broadleaved Natural Stands of Northeast China, Forests, 7(2),43, https://doi.org/10.3390/f7020043, 2016.

Lu, D., Mausel, P., Brondízio, E., and Moran, E.: Relationships between forest stand parameters and Landsat TM spectral responses in the Brazilian Amazon Basin, For Ecol Manage, 198, 149-167, https://doi.org/10.1016/j.foreco.2004.03.048, 2004.

645 Ma, Q., Su, Y., Niu, C., Ma, Q., Hu, T., Luo, X., Tai, X., Qiu, T., Zhang, Y., Bales, R. C., Liu, L., Kelly, M., and Guo, Q.: Tree mortality during long-term droughts is lower in structurally complex forest stands, Nat Commun, 14, 7467, 10.1038/s41467-023-43083-8, 2023.

Masaka, K., Sato, H., Torita, H., Kon, H., and Fukuchi, M.: Thinning effect on height and radial growth of *Pinus thunbergii Parlat*. trees with special reference to trunk slenderness in a matured coastal forest in Hokkaido, Japan, J For Res, 18, 475-481, https://doi.org/10.1007/s10310-012-0373-y, 2013.

Matasci, G., Hermosilla, T., Wulder, M. A., White, J. C., Coops, N. C., Hobart, G. W., and Zald, H. S. J.: Large-area mapping of Canadian boreal forest cover, height, biomass and other structural attributes using Landsat composites and lidar plots, Remote Sens Environ, 209, 90-106, https://doi.org/10.1016/j.rse.2017.12.020, 2018.

McGregor, I. R., Helcoski, R., Kunert, N., Tepley, A. J., Gonzalez-Akre, E. B., Herrmann, V., Zailaa, J., Stovall, A. E. L., Bourg, N. A., McShea, W. J., Pederson, N., Sack, L., and Anderson-Teixeira, K. J.: Tree height and leaf drought tolerance traits shape growth responses across droughts in a temperate broadleaf forest, New Phytol, 231, 601-616, https://doi.org/10.1111/nph.16996, 2021.

Mekruksavanich, S., Jantawong, P., Hnoohom, N., and Jitpattanakul, A.: Hyperparameter Tuning in Convolutional Neural Network for Face Touching Activity Recognition using Accelerometer Data, 2022 Research, Invention, and Innovation Congress: Innovative Electricals and Electronics (RI2C), Bangkok, Thailand, 4-5 Aug. 2022, 101-105, https://doi.org/10.1109/RI2C56397.2022.9910262, 2022

Migliavacca, M., Musavi, T., Mahecha, M. D., Nelson, J. A., Knauer, J., Baldocchi, D. D., Perez-Priego, O., Christiansen, R., Peters, J., Anderson, K., Bahn, M., Black, T. A., Blanken, P. D., Bonal, D., Buchmann, N., Caldararu, S., Carrara, A., Carvalhais, N., Cescatti, A., Chen, J., Cleverly, J., Cremonese, E., Desai, A. R., El-Madany, T. S., Farella, M. M., Fernández-Martínez, M., Filippa, G., Forkel, M., Galvagno, M., Gomarasca, U., Gough, C. M., Göckede, M., Ibrom, A., Ikawa, H., Janssens, I. A., Jung, M., Kattge, J., Keenan, T. F., Knohl, A., Kobayashi, H., Kraemer, G., Law, B. E., Liddell, M. J., Ma, X., Mammarella, I., Martini, D., Macfarlane, C., Matteucci, G., Montagnani, L., Pabon-Moreno, D. E., Panigada, C., Papale, D., Pendall, E., Penuelas, J., Phillips, R. P., Reich, P. B., Rossini, M., Rotenberg, E., Scott, R. L., Stahl, C., Weber, U., Wohlfahrt, G., Wolf, S., Wright, I. J., Yakir, D., Zaehle, S., and Reichstein, M.: The three major axes of terrestrial ecosystem function, Nature, 598, 468-472, 10.1038/s41586-021-03939-9, 2021.

Næsset, E.: Determination of mean tree height of forest stands using airborne laser scanner data, ISPRS J Photogramm Remote Sens, 52, 49-56, https://doi.org/10.1016/S0924-2716(97)83000-6, 1997.

Næsset, E. and Økland, T.: Estimating tree height and tree crown properties using airborne scanning laser in a boreal nature reserve, Remote Sens Environ, 79, 105-115, https://doi.org/10.1016/S0034-4257(01)00243-7, 2002.

Ni, X., Zhou, Y., Cao, C., Wang, X., Shi, Y., Park, T., Choi, S., and Myneni, R. B.: Mapping Forest Canopy Height over Continental China Using Multi-Source Remote Sensing Data, Remote Sensing, https://doi.org/10.3390/rs70708436, 2015.

Ørka, H. O., Næsset, E., and Bollandsås, O. M.: Classifying species of individual trees by intensity and structure features derived from airborne laser scanner data, Remote Sens Environ, 113, 1163-1174, https://doi.org/10.1016/j.rse.2009.02.002, 2009.

Pang, Y., Zhao, F., and Li, Z.: Forest height inversion using airborne Lidar technology, Journal of Remote Sensing, 12, 158, 10.11834/jrs.20080120 ,2008.

Potapov, P., Li, X., Hernandez-Serna, A., Tyukavina, A., Hansen, M. C., Kommareddy, A., Pickens, A., Turubanova, S., Tang, H., Silva, C. E., Armston, J., Dubayah, R., Blair, J. B., and Hofton, M.: Mapping global forest canopy height through integration of GEDI and Landsat data, Remote Sens Environ, 253, 112165, https://doi.org/10.1016/j.rse.2020.112165, 2021.

685 Qin, H., Zhou, W., Yao, Y., and Wang, W.: Individual tree segmentation and tree species classification in subtropical broadleaf forests using UAV-based LiDAR, hyperspectral, and ultrahigh-resolution RGB data, Remote Sens Environ, 280, 113143, https://doi.org/10.1016/j.rse.2022.113143, 2022.

Saatchi, S. S., Harris, N. L., Brown, S., Lefsky, M., Mitchard, E. T. A., Salas, W., Zutta, B. R., Buermann, W., Lewis, S. L., Hagen, S., Petrova, S., White, L., Silman, M., and Morel, A.: Benchmark map of forest carbon stocks in tropical regions across

690 three continents, Proceedings of the National Academy of Sciences, 108, 9899-9904, 10.1073/pnas.1019576108, 2011.

Simard, M., Pinto, N., Fisher, J. B., and Baccini, A.: Mapping forest canopy height globally with spaceborne lidar, J Geophys Res Biogeosci, 116, https://doi.org/10.1029/2011JG001708, 2011.

Su, Y., Ma, Q., and Guo, Q.: Fine-resolution forest tree height estimation across the Sierra Nevada through the integration of spaceborne LiDAR, airborne LiDAR, and optical imagery, Int J Digit Earth, 10, 307-323,

695 https://doi.org/10.1080/17538947.2016.1227380, 2017.

Su, Y., Guo, Q., Ma, Q., and Li, W.: SRTM DEM Correction in Vegetated Mountain Areas through the Integration of Spaceborne LiDAR, Airborne LiDAR, and Optical Imagery, Remote Sensing, https://doi.org/10.3390/rs70911202, 2015.

Swayze, N. C., Tinkham, W. T., Vogeler, J. C., and Hudak, A. T.: Influence of flight parameters on UAS-based monitoring of tree height, diameter, and density, Remote Sens Environ, 263, 112540, https://doi.org/10.1016/j.rse.2021.112540, 2021.

700 Tang, J., Luyssaert, S., Richardson, A. D., Kutsch, W., and Janssens, I. A.: Steeper declines in forest photosynthesis than respiration explain age-driven decreases in forest growth, Proc Natl Acad Sci U S A, 111, 8856-8860, https://doi.org/10.1073/pnas.1320761111, 2014.

Tao, S., Wu, F., Guo, Q., Wang, Y., Li, W., Xue, B., Hu, X., Li, P., Tian, D., Li, C., Yao, H., Li, Y., Xu, G., and Fang, J.: Segmenting tree crowns from terrestrial and mobile LiDAR data by exploring ecological theories, ISPRS J Photogramm

705 Remote Sens, 110, 66-76, https://doi.org/10.1016/j.isprsjprs.2015.10.007, 2015.

Travers-Smith, H., Coops, N. C., Mulverhill, C., Wulder, M. A., Ignace, D., and Lantz, T. C.: Mapping vegetation height and identifying the northern forest limit across Canada using ICESat-2, Landsat time series and topographic data, Remote Sens Environ, 305, 114097, https://doi.org/10.1016/j.rse.2024.114097, 2024.

Vaglio Laurin, G., Ding, J., Disney, M., Bartholomeus, H., Herold, M., Papale, D., and Valentini, R.: Tree height in tropical

710 forest as measured by different ground, proximal, and remote sensing instruments, and impacts on above ground biomass estimates, Int J Appl Earth Obs Geoinf, 82, 101899, https://doi.org/10.1016/j.jag.2019.101899, 2019.

Vanclay, J. K.: Assessing site productivity in tropical moist forests: a review, For Ecol Manage, 54, 257-287, https://doi.org/10.1016/0378-1127(92)90017-4, 1992.

Vatandaslar, C., Narin, O. G., and Abdikan, S.: Retrieval of forest height information using spaceborne LiDAR data: a comparison of GEDI and ICESat-2 missions for Crimean pine (Pinus nigra) stands, Trees, 37, 717-731, https://doi.org/10.1007/s00468-022-02378-x, 2023.

Wang, M., Kane, M. B., and Zhao, D.: Correlation-Regression Analysis for Understanding Dominant Height Projection Accuracy, Forest Science, 69, e1-e10, https://doi.org/10.5849/fs-2016-092, 2023.

Wang, Y., Pyörälä, J., Liang, X., Lehtomäki, M., Kukko, A., Yu, X., Kaartinen, H., and Hyyppä, J.: In situ biomass estimation at tree and plot levels: What did data record and what did algorithms derive from terrestrial and aerial point clouds in boreal forest, Remote Sens Environ, 232, 111309, https://doi.org/10.1016/j.rse.2019.111309, 2019a.

Wang, Y., Lehtomäki, M., Liang, X., Pyörälä, J., Kukko, A., Jaakkola, A., Liu, J., Feng, Z., Chen, R., and Hyyppä, J.: Is field-measured tree height as reliable as believed – A comparison study of tree height estimates from field measurement, airborne laser scanning and terrestrial laser scanning in a boreal forest, ISPRS J Photogramm Remote Sens, 147, 132-145, https://doi.org/10.1016/j.isprsjprs.2018.11.008, 2019b.

Woods, M., Pitt, D., Penner, M., Lim, K., Nesbitt, D., Etheridge, D., and Treitz, P.: Operational implementation of a LiDAR inventory in Boreal Ontario, The Forestry Chronicle, 87, 512-528, https://doi.org/10.5558/tfc2011-050, 2011.

Wu, Z. and Shi, F.: Mapping Forest Canopy Height at Large Scales Using ICESat-2 and Landsat: An Ecological Zoning Random Forest Approach, IEEE Trans Geosci Remote Sens, 61, 1-16, https://doi.org/10.1109/TGRS.2022.3231926, 2023.

Xu, H., Yue, C., Zhang, Y., Liu, D., and Piao, S.: Forestation at the right time with the right species can generate persistent carbon benefits in China, Proc Natl Acad Sci U S A, 120, e2304988120, https://doi.org/10.1073/pnas.2304988120, 2023.

Xu, Y., Li, C., Sun, Z., Jiang, L., and Fang, J.: Tree height explains stand volume of closed-canopy stands: Evidence from forest inventory data of China, For Ecol Manage, 438, 51-56, https://doi.org/10.1016/j.foreco.2019.01.054, 2019.

Yang, J., Kang, Z., Cheng, S., Yang, Z., and Akwensi, P. H.: An Individual Tree Segmentation Method Based on Watershed Algorithm and Three-Dimensional Spatial Distribution Analysis From Airborne LiDAR Point Clouds, IEEE J Sel Top Appl Earth Obs Remote Sens, 13, 1055-1067, https://doi.org/10.1109/JSTARS.2020.2979369, 2020.

Yang, Q., Niu, C., Liu, X., Feng, Y., Ma, Q., Wang, X., Tang, H., and Guo, Q.: Mapping high-resolution forest aboveground biomass of China using multisource remote sensing data, GIsci Remote Sens, 60, 2203303, https://doi.org/10.1080/15481603.2023.2203303, 2023.

Yang, Z., Su, Y., Li, W., Cheng, K., Guan, H., Ren, Y., Hu, T., Xu, G., and Guo, Q.: Segmenting Individual Trees From Terrestrial LiDAR Data Using Tree Branch Directivity, IEEE J Sel Top Appl Earth Obs Remote Sens, 17, 956-969, https://doi.org/10.1109/JSTARS.2023.3334014, 2024.

Yao, Y., Piao, S., and Wang, T.: Future biomass carbon sequestration capacity of Chinese forests, Science Bulletin, 63, 1108-1117, https://doi.org/10.1016/j.scib.2018.07.015, 2018.

Yin, D., Wang, L., Lu, Y., and Shi, C.: Mangrove tree height growth monitoring from multi-temporal UAV-LiDAR, Remote Sens Environ, 303, 114002, https://doi.org/10.1016/j.rse.2024.114002, 2024.

Yun, T., Jiang, K., Li, G., Eichhorn, M. P., Fan, J., Liu, F., Chen, B., An, F., and Cao, L.: Individual tree crown segmentation from airborne LiDAR data using a novel Gaussian filter and energy function minimization-based approach, Remote Sens Environ, 256, 112307, https://doi.org/10.1016/j.rse.2021.112307, 2021.

750   Zemp, D. C., Guerrero-Ramirez, N., Brambach, F., Darras, K., Grass, I., Potapov, A., Röll, A., Arimond, I., Ballauff, J., Behling, H., Berkelmann, D., Biagioni, S., Buchori, D., Craven, D., Daniel, R., Gailing, O., Ellsäßer, F., Fardiansah, R., Hennings, N., Irawan, B., Khokthong, W., Krashevska, V., Krause, A., Kückes, J., Li, K., Lorenz, H., Maraun, M., Merk, M. S., Moura, C. C. M., Mulyani, Y. A., Paterno, G. B., Pebrianti, H. D., Polle, A., Prameswari, D. A., Sachsenmaier, L., Scheu, S., Schneider, D., Setiajiati, F., Setyaningsih, C. A., Sundawati, L., Tscharntke, T., Wollni, M., Hölscher, D., and Kreft, H.:

755   Tree islands enhance biodiversity and functioning in oil palm landscapes, Nature, 618, 316-321, 10.1038/s41586-023-06086-5, 2023.

Zhang, G., Ganguly, S., Nemani, R. R., White, M. A., Milesi, C., Hashimoto, H., Wang, W., Saatchi, S., Yu, Y., and Myneni, R. B.: Estimation of forest aboveground biomass in California using canopy height and leaf area index estimated from satellite data, Remote Sens Environ, 151, 44-56, https://doi.org/10.1016/j.rse.2014.01.025, 2014.

760   Zhao, X., Su, Y., Hu, T., Cao, M., Liu, X., Yang, Q., Guan, H., Liu, L., and Guo, Q.: Analysis of UAV lidar information loss and its influence on the estimation accuracy of structural and functional traits in a meadow steppe, Ecological Indicators, 135, 108515, https://doi.org/10.1016/j.ecolind.2021.108515, 2022.